NASA CR-145095

SAI-76-717-LJ
March 30, 1977

Contract No. NAS1-13573

AIRBORNE HCL - CO SENSING SYSTEM

FINAL REPORT

SCIENCE APPLICATIONS, INC.
1200 Prospect Street
La Jolla, California 92037

By: E. R. Bartle
Gordon Hall

Prepared For:

NASA
National Aeronautics and
Space Administration

FOREWORD

This report summarizes the research and development performed under Contract NAS1-13573 between October, 1974 and March 1977. The work was sponsored by the National Aeronautics and Space Administration, Langley Research Center, Hampton, Virginia. The technical monitors for the program were W. S. Lassiter and D. E. Wornom. The object of this program was to develop an aircraft borne sensor system that could traverse the effluent cloud from a rocket exhaust and provide in-situ measurements of the Hydrochloric Acid and Carbon Monoxide gases in the cloud.

The authors of this report are indebted to E. A. Meckstroth, and G. K. Houghton for their valuable contributions in the design, fabrication and testing of the system.

TABLE OF CONTENTS

SUMMARY

A system for measuring air pollutants in-situ using an aircraft was designed, fabricated and tested. The system is based upon a technique called Gas Filter Correlation (GFC) which provides for high sensitivity and specificity in the presence of interfering species. This particular system was designed for measuring hydrochloric acid and carbon monoxide gases emitted from rocket exhaust effluents.

The GFC technique is based upon Non-Dispersive-Infra-Red spectroscopy. HC1 and CO gases are an integral part of the sensor system and provide a selective filter for their detection.

The system was designed so that the sensor portion was located inside the aircraft cabin and a uniquely designed retroreflector was located on the wing tip. Thus, as the aircraft passes through a pollution cloud, integrated measurements of the concentrations are given.

Final performance checks of the system gave sensitivities of less than two parts per million with a one-half second response time.

The system was test flown several times and proved to be extremely stable (in signal) over a wide range of temperatures in the aircraft. A data flight provided information on the concentrations of HC1 and CO emitted from a Titan III missile.

Following the data flight the instrument was returned to SAI for further evaluation.

LIST OF FIGURES

LIST OF FIGURES (Contd.)

LIST OF TABLES

1.0 INTRODUCTION

The exhaust from solid rocket motors contains large quantities of HCl and CO which are of concern because of potential reactivity. HCl gas is toxic above about 5 ppm; in addition, it combines with water, which is present in the exhaust, to form the corrosive HCl acid. It is important to monitor the interaction of these gases with the atmosphere after release by the solid rocket motor. Certain theoretical models exist, but these must be confirmed with measured data. Accurate three-dimensional real-time mapping of the exhaust cloud as it mixes with the atmosphere is needed, and is best accomplished with an optical instrument on an aircraft which can fly through the exhaust cloud.

The use of optical techniques for real-time monitoring is attractive since they do not require a sampling system that degrades accuracy and affects response times. The principle of optical measurements is based upon the fact that most gases absorb energy at specific wavelengths. Thus, optical measurement techniques are only limited in response time due to the response characteristics of the detector and the data integration time.

In recent years a number of optical techniques have been developed for detecting gaseous pollutants. These include infrared absorption spectrometers, Raman scattering systems, fluorescent systems, laser absorption and differential absorption systems, and optical correlation techniques.

Studies (1, 2) have been conducted to evaluate all optical techniques for detection of air pollutants. It was found that the techniques best suited are those that utilize the spectral fine-structure of pollutants with a preselected instrument transfer function to enhance specificity. As shown in the next section, specificity is a strong requirement for optical measurements.

Among the various optical techniques is one called Gas Filter Correlation (GFC) which has been used for a number of prototype systems.[3-6] It is based upon the Non-Dispersive-Infrared (NDIR) technique that makes use of the particular gas to be detected to provide specificity.

The first detailed description of an NDIR instrument was given by Luft[7], although elements of the techniques were mentioned already by Pfund[8] in 1939. Two different light-sources, two cells and one membrane condenser detector were used. The detector was sensitized with the gas of interest. This method, using a sensitized detector and the gas sample in one light beam, was later classified as "positive filtering".

A different arrangement by Schmick[9] and Wright and Herscher[10] used one light source, but two cells and two detectors, which were the two opposed arms of an ac excited bolometer. In this case, the selectivity is provided by balancing the two cells, and the detectors are non-selective. The gas sample is introduced into a cell common to both light beams. This was later classified as a "negative filtering".

GFC is based upon absorption or emission of electromagnetic energy by the specific pollutant to be monitored. As such, GFC can operate in the UV, visible, or IR regions of the spectrum. The IR may be preferable because all pollutants of interest have rotational lines that absorb in the IR; also scattering effects are more pronounced in the UV and visible. On the other hand, the UV-visible may be preferable if extreme spectral interferences occur in the IR; also, more sensitive photomultiplier detectors are available and pollutant absorptivities are greater.

Conventional spectroscopic instruments depend upon finding a single absorption line of a particular species. GFC makes use of the contribution of all absorption lines of a band system of a particular species.

The GFC signal is a function both of the concentration of the pollutant species in the test sample, and of the degree of correlation between its spectrum and the spectrum of the pollutant of interest. When these species are the same, the correlation coefficient is unity.

Specificity is obtained because of random correlation between spectra of the particular species and interfering species; the principle of random correlation has been established for most pollutant species and interfering species occurring naturally and in polluted atmospheres. In addition, a ratioing technique may be employed that minimizes effects of changes in source intensity, background radiation, and continuum absorption due to complex molecules, aerosols, or water vapor.

The GFC technique can be applied to both double and single ended systems. For the double ended system, an active infrared source and GFC receiver are used to measure an intervening pollutant; in this case, the detection principle is based upon absorption spectroscopy. For the single ended system, only the GFC receiver is used to remotely detect a pollutant; in this case, the detection principle is based upon either emission or absorption spectroscopy depending upon the relative temperatures of the pollutant to be detected and the background. In this report, the development and testing of a two channel double ended GFC system for simultaneous monitoring of HC1 and CO is described. This sytem consists of a sensor located inside the aircraft and a Corner Reflector Array, mounted externally on the wing-tip fuel tank (see Figure 1-1).

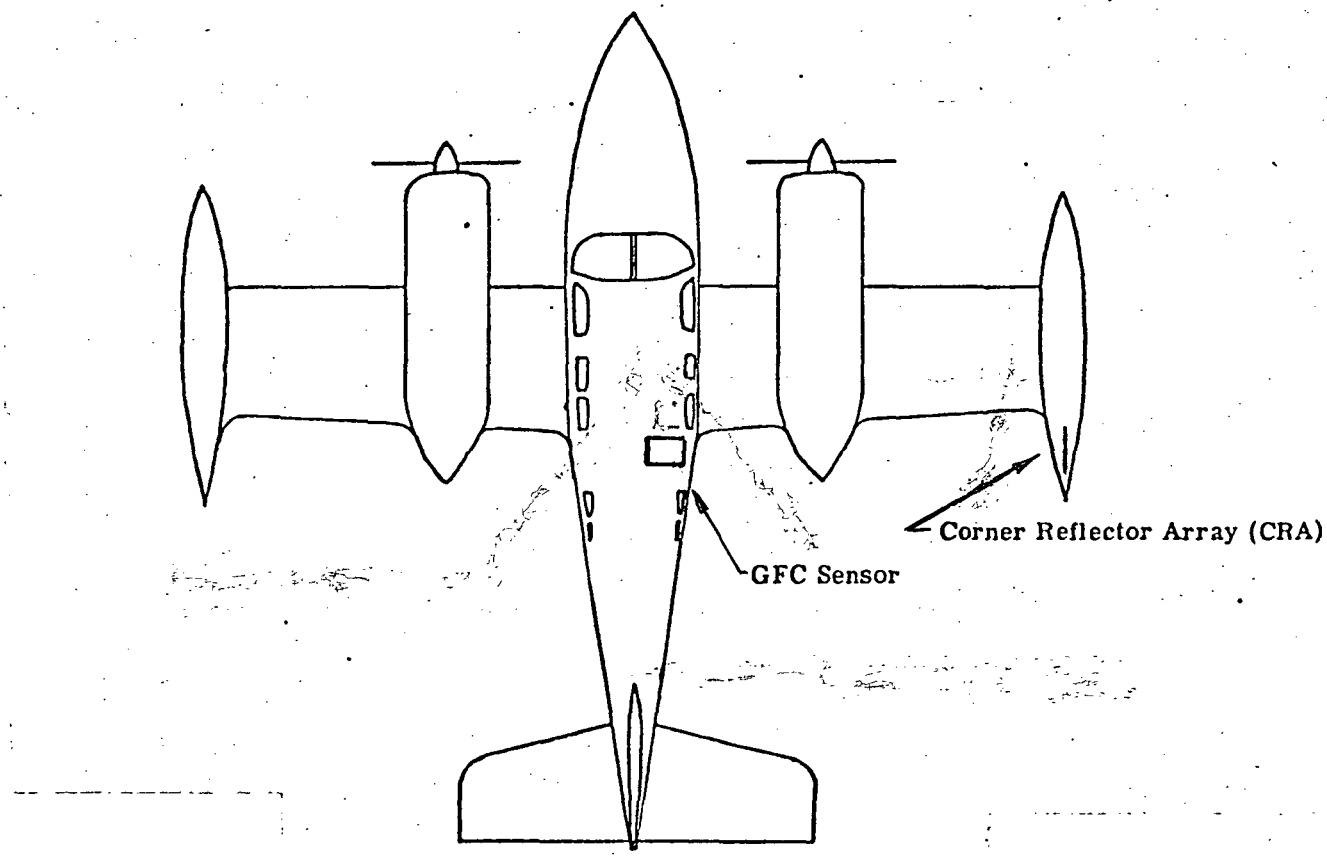

Figure 1-1. Outline Drawing of Cessna 402 Aircraft Locations of Sensor and CRA

2.0 DESIGN OBJECTIVES AND CONSTRAINTS

The basic design objectives and constraints are:

System	-	Optical instrument using a sensing path external to a Cessna 402 aircraft.
Sensitivity	-	0.25-1 ppm with 90% response in less than 10 sec. 1-500 ppm with 90% response in less than 0.5 sec.
Specificity	-	Effects due to interfering species to be less than 250 ppb.
Accuracy	-	$\pm$5 percent of reading.
Power	-	110 volts, 400 Hz or 28 volts DC.
Performance	-	No reduction in accuracy when operating in aircraft environment.

Optical measurements made from an aircraft impose severe requirements on the sensor. The major problem is due to vibration that can affect the optical alignment of the sensor. Of secondary concern is the thermal environment that can also affect the optical alignment. Any optics that are mounted external to the aircraft require special consideration. A design that is insensitive to optical misalignment caused by vibrations is mandatory.

In addition to HCl and CO, rocket exhaust emissions may contain large amounts of the gases CO_2, H_2O and particulate Al_2O_3. Also present in the polluted atmosphere may be NO, NO_2, O_3, SO_2, CH_4 and N_2O. Any or all of these gases can affect optical measurements. Figure 2-1 shows the spectral locations and relative band absorption coefficients for the listed species.

From Figure 2-1, it is apparent that in the measurement of (1) HCl, interferences may result from the presence of CH_4, O_3 and NO_2; and (2) CO, interferences may result from the presence of N_2O Al_2O_3 particles and the H_2O continuum extend over the entire spectrum and may affect the measurements.

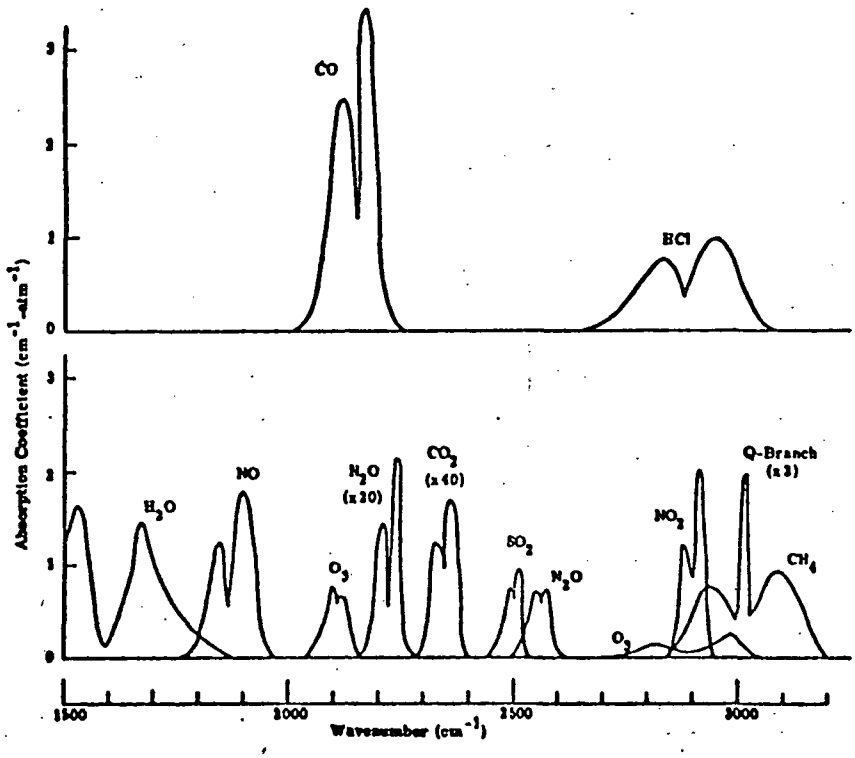

Figure 2-1.

Band Spectra of HCl and CO and Interfering Gases

In view of the above discussion, initial laboratory experiments were conducted prior to the building of the flight system to establish performance characteristics.

3.0 LABORATORY EXPERIMENTS

Experiments were conducted to establish the sensitivity and specificity characteristics of GFC for detecting HCl and CO, using existing breadboard sensors, and to test a newly developed Corner Reflector Array (CRA) to establish its sensitivity to optical alignment.

3.1 Description of Breadboard Sensors

The theory underlying the GFC technique has been described in detail,[3-6] and is expanded in Appendix A. Basically, it consists of mechanically chopping an infrared source of radiation alternately between a gas cell containing the species to be detected and a reference cell which has no absorption in the spectral region of interest. The AC signal, due to a gaseous mixture containing the species to be detected, is the correlated signal and is expressed by ΔV. By mechanically chopping the average infrared radiance passing through the two cells at a different frequency, a second AC signal, expressed by V is generated. Electronic ratioing gives a $\Delta V/V$ signal that eliminates variations in output responsivity and neutral attenuations in the optical path.

Figure 3-1 is a schematic drawing of the breadboard system. The optical system consists of a source aperture which is imaged by the source lens onto the detector lens, and a detector lens which images the source lens (cell mask) onto the detector.

High frequency chopping (ΔV) is performed by a tuning fork chopper at 200 Hz and the low frequency chopping at 12.6 Hz with a mirrored surface facing the source. This is done to reduce the effects of temperature changes of the chopper blade on the V signal. Both choppers are located at the source end of the instrument to minimize the number of components which have chopped emission.

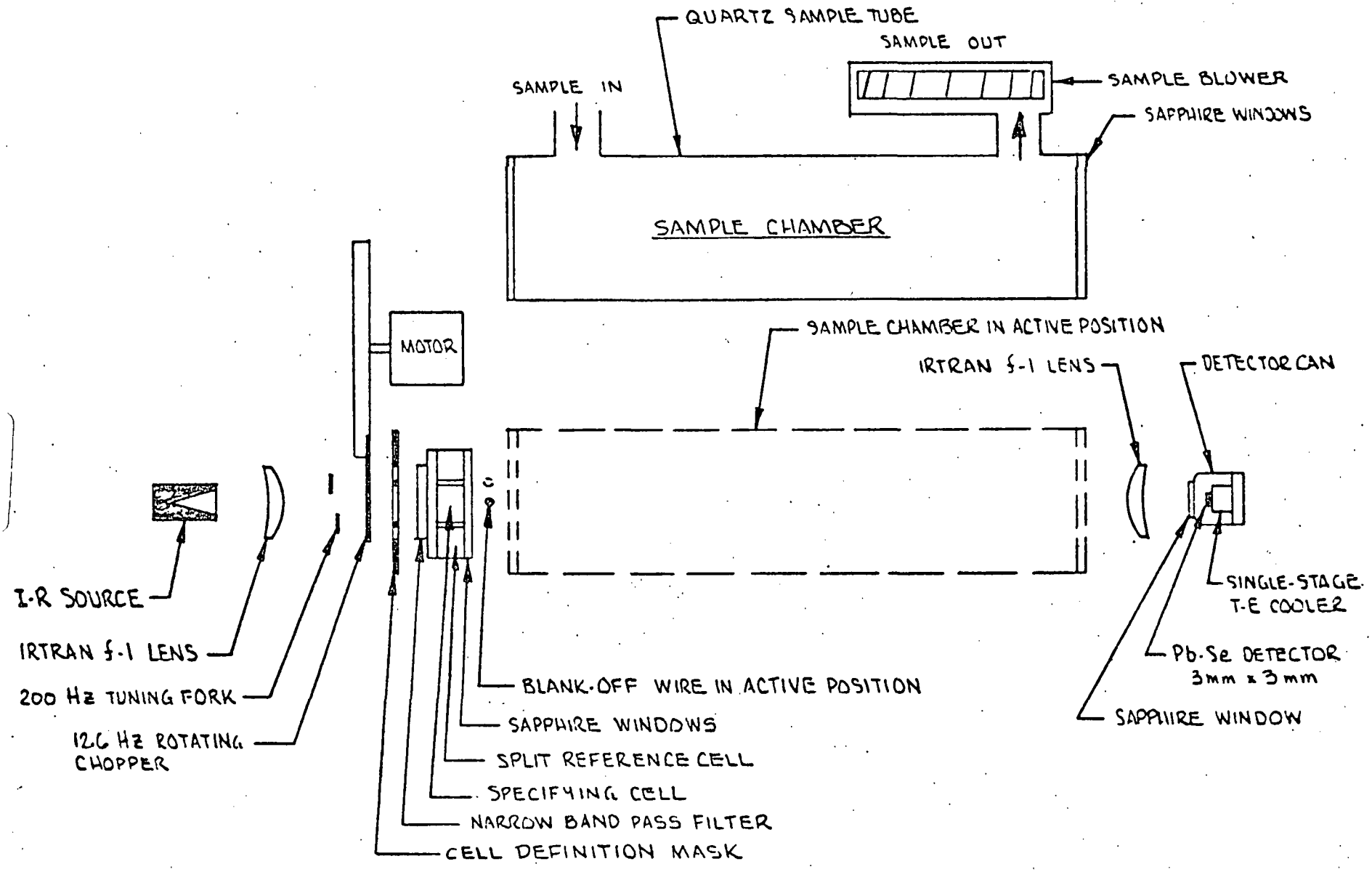

Figure 3-1. Optical System Schematic, Breadboard System

The source aperture required is 3.3 mm but is oversized to accommodate any slight motions of the source due to thermal expansion of the support structure near the high-temperature source. The source requires less than 20 W to achieve a 1200 K temperature. It is a cone-shaped cavity to ensure temperature uniformity.

The detector (3 x 3 mm PbSe) is located on a single-stage thermoelectric cooler to achieve an operating temperature of 280 K and is temperature regulated to 0.3 K. The high degree of regulation minimizes responsivity changes during operation.

The quartz sample cell is 20 cm long and may be removed for true in-situ operation.

A blank-off wire can be inserted into the reference cell fov. This provides for a span reference calibration by mechanically creating a fixed offset in the ΔV signal equivalent to 500 ppm HCl. Zeroing is done electronically.

Figure 3-2 gives a simplified block diagram of the electronics system used in the unit. Infrared radiation chopped at two frequencies, f_1 (cell chopper) and f_2 (source chopper) falls upon the temperature stabilized PbSe detector. The output of the detector is amplified with a low-noise pre-amplifier and additional stages of amplification, and then is split into inputs to the ΔV and V channels.

The ΔV input is passed through a bandpass filter to remove the f_2 component of the signal. The output of the filter is then fed to span and range amplifiers which respectively adjust the magnitude of the signal for full scale span and the measuring range of the instrument output. The output of the range amplifier is fed into four gated sample and hold systems, which sample different but specific parts of the input signal according to triggering inputs from the data gates.

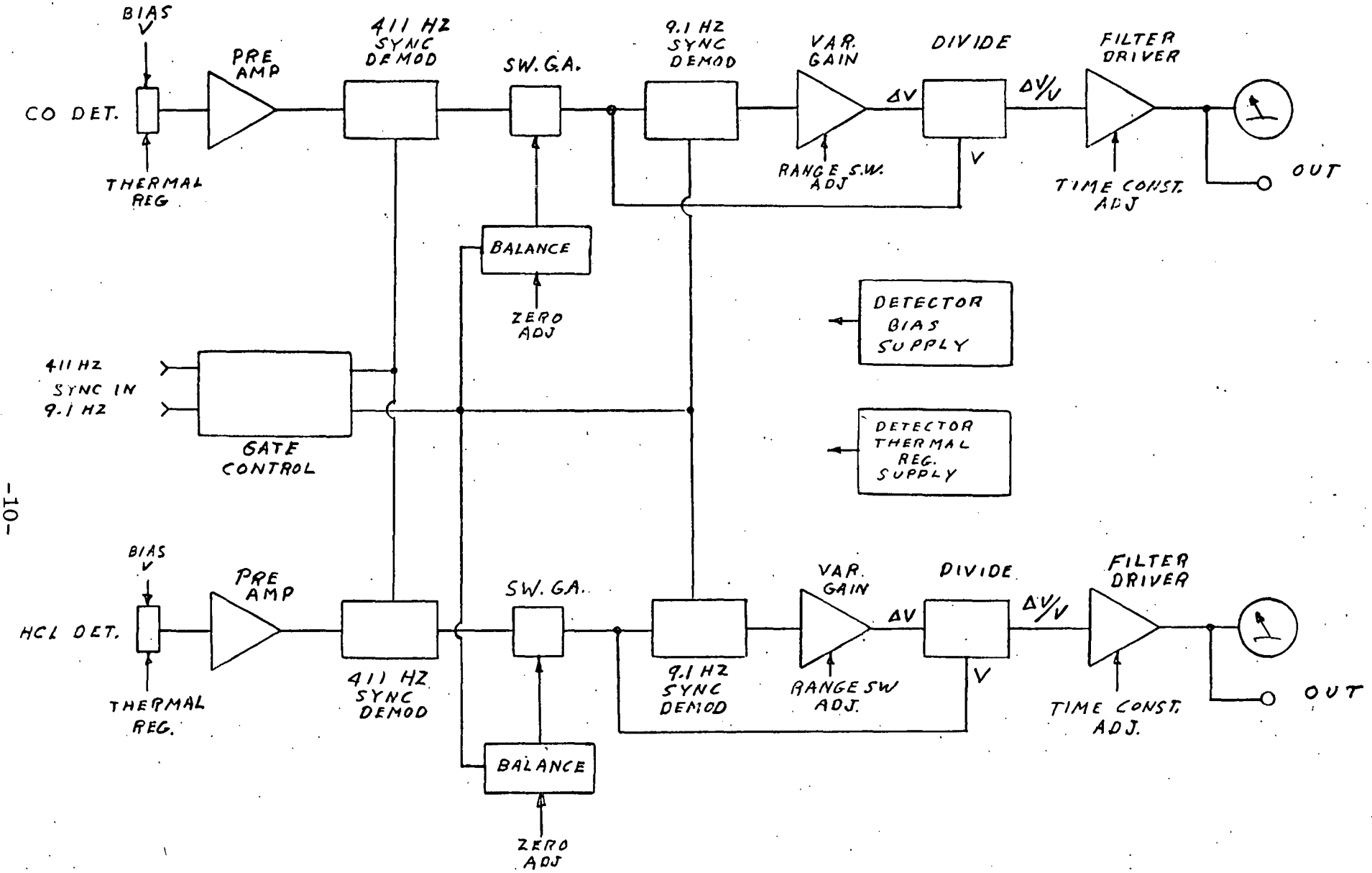

Figure 3-2. Electronics Block Diagram

These four sampled data points are the positive and negative peaks of the 200 Hz and 12.6 Hz waveforms from which the peak-to-peak amplitudes are obtained. Although the 200 Hz is superimposed on the 12.6 Hz signal, the 200 Hz has a small amplitude compared to that of the lower frequency and so causes a negligible error in its measured amplitude.

The outputs of the unit are ΔV, V, and $\Delta V/V$, where the $\Delta V/V$ signal is derived by applying the ΔV and V signals to an analogue divider. The display is a panel meter. Additionally, a jack for a strip chart recorder is provided.

3.2 Design Performance

The pollutant-generated signal, referred to the instrument detector, is closely given by:

$$S = \Delta V = \eta A \Omega N^{O} \tau_{o} \bar{k} C L p \Delta\lambda R, \text{ volts} \qquad (3\text{-}1)$$

where

- η is the overall efficiency
- A is the area of the specifying cell
- Ω is the solid angle subtended by the detector lens
- N^{O} is the blackbody source radiance
- τ_{o} is the specifying-cell transmissivity
- $\bar{k}$ is the mean absorption coefficient
- C is the concentration
- L is the optical pathlength
- p is the sample pressure
- $\Delta\lambda$ is the filter HBW
- R is the detector responsivity

For a detector-noise limited system, the root mean square (rms) noise, at the detector is

$$N_{rms} = \frac{\sqrt{A_d \, \Delta f}}{D^*} R, \text{ volts} \qquad (3\text{-}2)$$

where

A_d is the detector area
Δf is the electronics-noise bandpass
D* is the specific detectivity
R is the detector responsivity

The values of the breadboard instrument parameters for measuring HC1 and CO are presented in Table 1.

From the instrument parameter values given in Table 1 and the signal and noise equations, it is calculated that the minimum detectabilities for HC1 and CO are 39 and 25 ppb, respectively. If, however, the minimum detectability is defined by $S/N_{p-p} = 1$, where N_{p-p} is the peak-to-peak noise, the minimum dectabilities will be higher by a factor of 5; i.e., 195 and 125 ppb for HC1 and CO, respectively.

3.3 HC1 Experimental Results

3.3.1 Sensitivity

Measurements were made of the relative signal, using 100 ppm HC1 diluted with N_2 to 1 atm pressure in the sample cell with varying HC1 concentrations in the specifying cell. These results indicated optimum sensitivity is obtained for a specifying cell transmissivity τ_o(0.8 to 0.9). Thus, a $\tau_o = 0.9$ was used for the final sensitivity and specificity experiments.

Measurements of the signal and noise for N_2-diluted mixtures of HC1 were made. The results are shown in Figure 3-3.

Using the system gain factor given in Table 1 and the signal equation, the theoretical signal calculated for 10 ppm HC1 is 1.9V compared with the 2.0V measured.

TABLE 1. SUMMARY OF BREADBOARD INSTRUMENT PARAMETERS

Parameter	HCl	CO	Note
η	0.031	0.031	a
A, cm^2	2.16	2.16	--
Ω, sr	0.012	0.012	b
$N^o(T = 1000^oC)$, W/cm^2-μ-sr	0.47	0.26	c
τ_o	0.90	0.83	d
$\bar{k}$, $atm^{-1}cm^{-1}$	0.50	1.5	e
L, cm	20.0	20.0	--
P, atm	1.0	1.0	--
$\Delta\lambda$, μm	0.18	0.20	f
R, V/W	1.05×10^4	1.6×10^4	g
A_d, cm^2	0.09	0.09	--
Δf, Hz	0.025	0.025	h
D*, cm $Hz^{1/2}/W$	2.0×10^9	1.8×10^9	i
S (C=1), V	6.42	16.65	--
N_{rms}, V	2.5×10^{-7}	4.2×10^{-7}	--
C_{min}	39 ppb	25 ppb	j
System Gain	3×10^4	6×10^4	k

[a] η is assumed to be the product of the transmissivities of the two lenses (τ_L), the two cell windows (τ_W), the two sample-cell windows (τ_S), the gas transmissivity (τ_o'), the emissivity of the source (ε_S), the optical filter (τ_F), and the electronics efficiency (η_e); viz

$$\eta = (\tau_L)^2(\tau_W)^2(\tau_S)^2(\tau_o')(\varepsilon_S)(\tau_F)(\eta_e) \qquad (3\text{-}3)$$

$$= (.75)^2(.88)^2(.88)^2(.9)(.5)(.65)(.31)$$

$$= .031$$

[b] $\Omega = \pi \sin^2\alpha \simeq \pi(\frac{1.25}{20})^2$

[c] For HCl, λ_o = 3.4 μm, and for CO, λ_o = 4.7 μm.

[d] Based on measured values with the pertinent optical filters.

[e] Same as note d.

[f] Uses actual optical filter HBW.

[g] Actual measured responsivity of the detector at operating temperature of 20^oC.

[h] $\Delta f = 1/4t$ where t is the time constant to reach 63% of full scale (=10 seconds).

[i] Actual detector D* at 200 Hz and $T = 20^oC$.

[j] C_{min} is minimum detectable concentration for $S/N_{rms} = 1$.

[k] Overall electronic gain applied to detector output.

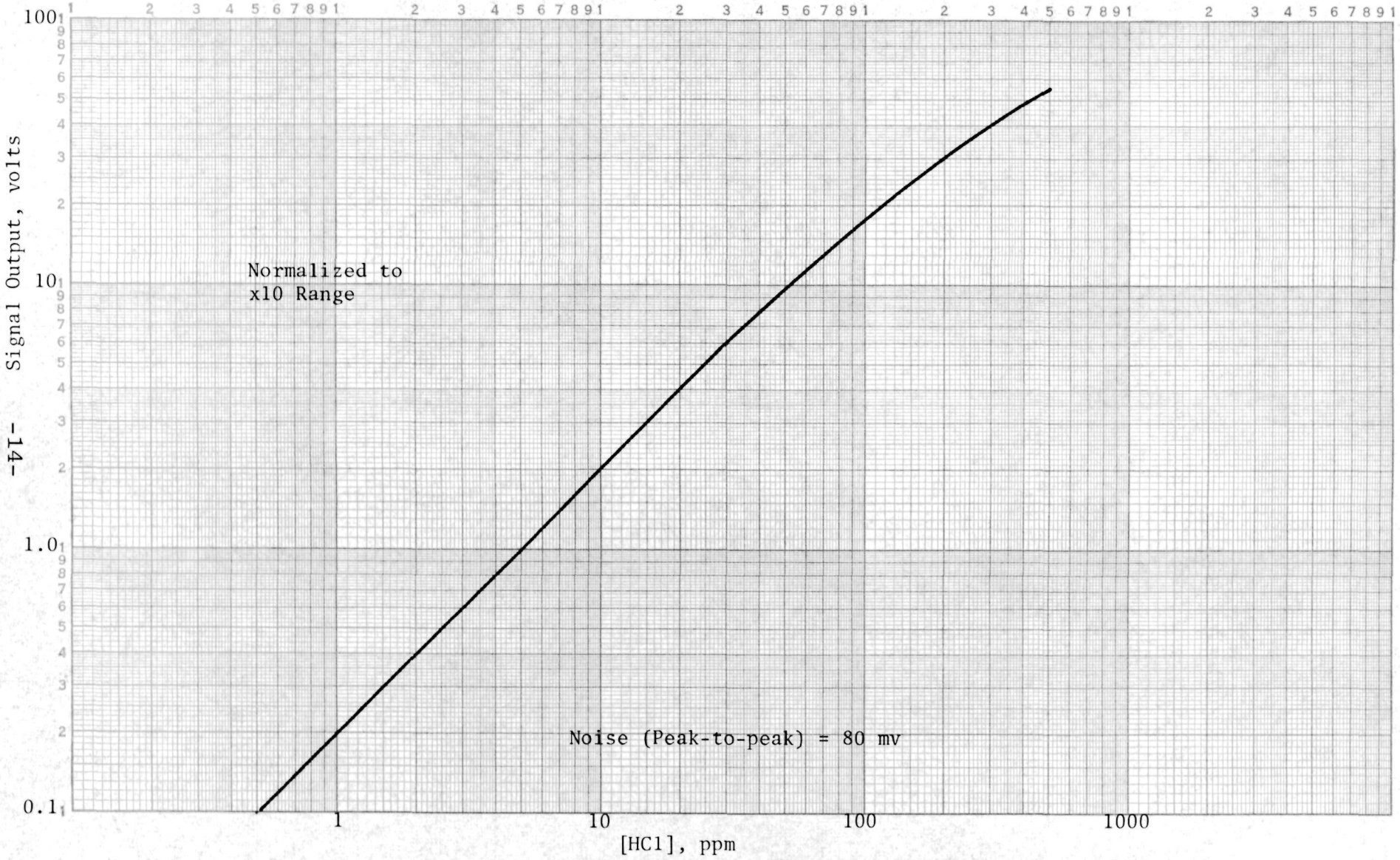

Figure 3-3. Output Response For 20 cm Optical Pathlength GFC Gas Analyzer to N_2 Diluted HCl

Correspondingly, the calculated peak-to-peak noise is 30 mV, compared with the 80 mV measured. This indicates a sensitivity of about 0.4 ppm HC1.

3.3.2 Specificity

Measurements were made of the effects due to the presence of CH_4, CO and H_2O. The results are shown below.

Experiment	Results
HC1 + CH_4	1.4 ppm CH_4 → <0.4 ppm HC1
HC1 + CO	100 ppm CO → no effect.
HC1 + H_2O	3.5% H_2O (= 100% R.H. at 300K) → <0.4 ppm HC1

Theoretical calculations were made using a spectral line-by-line computer program assuming 20 cm and 8 m path lengths. The results are shown in Figures 3-4 and 3-5 and the 8 m path length results re-plotted linearly (see Figure 3-6). It appears that the theoretical calculations are overly pessimistic since measurements with 3.5 percent water vapor indicate less than a 0.4 ppm effect, while the theoretical calculations indicate a 1.2 ppm effect.

3.4 CO Experimental Results

3.4.1 Sensitivity

Measurements were made using CO similar to those discussed for HC1 in Section 3.3.1. It turns out that for CO the optimum τ_o is 0.80 to 0.85 and, thus, $\tau_o = 0.83$ was used for the final experiments.

The measurements of the signal and noise for N_2-diluted mixtures of CO are presented in Figure 3-7.

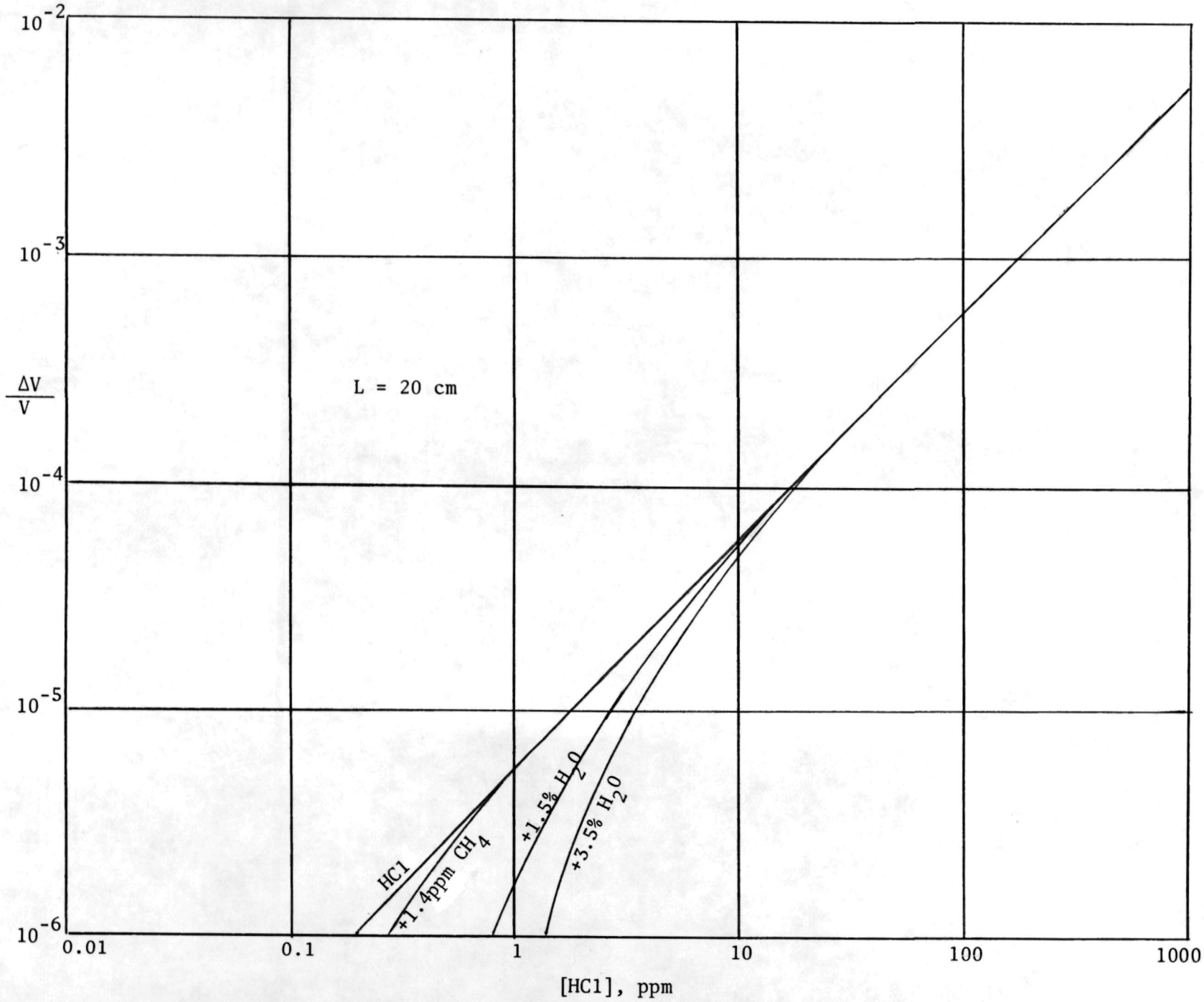

Figure 3-4. Theoretical Influence of Interfering Species on HCl for L = 20cm

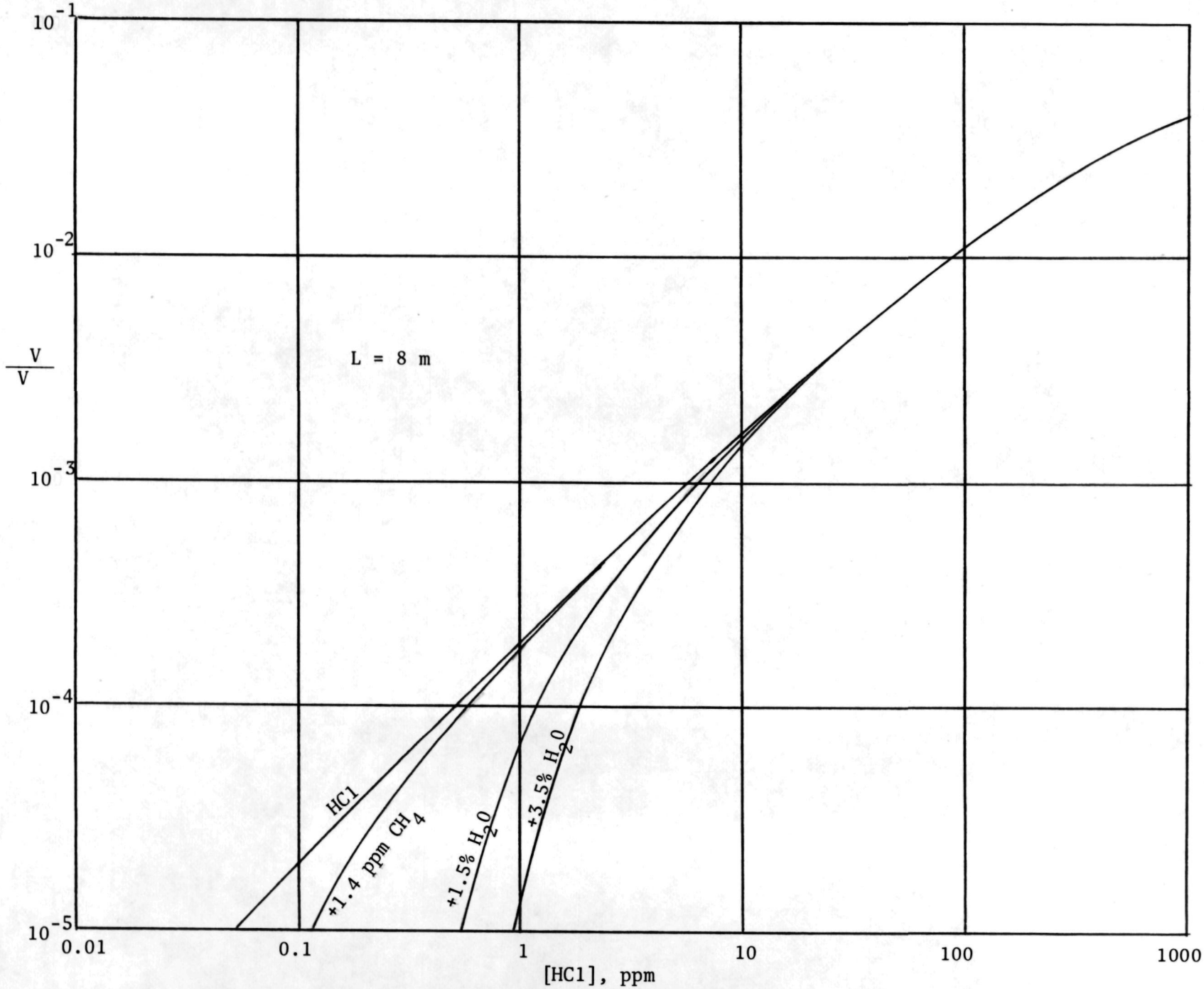

Figure 3-5. Theoretical Influence of Interfering Species on HCl for L = 8m

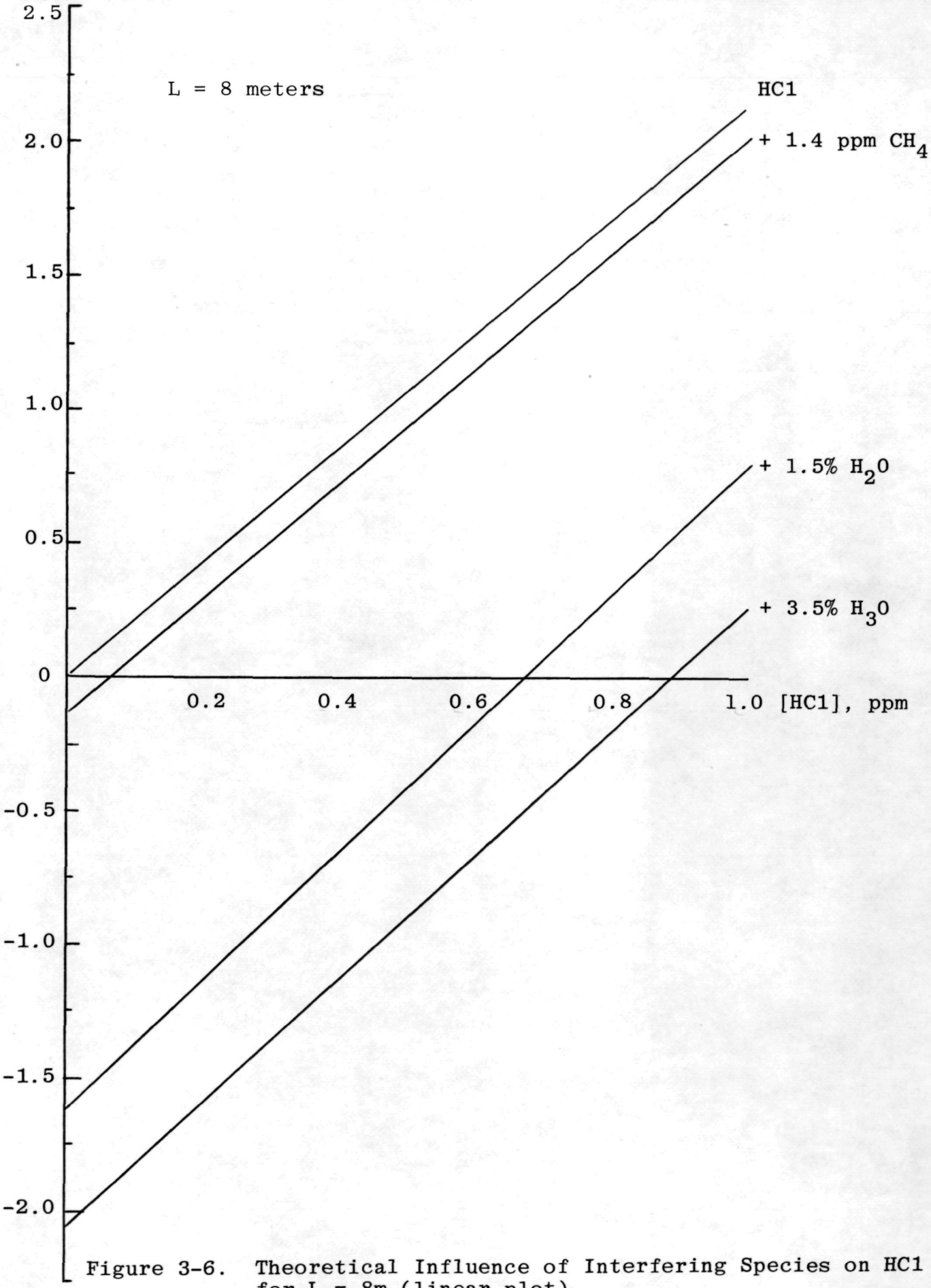

Figure 3-6. Theoretical Influence of Interfering Species on HC1 for L = 8m (linear plot)

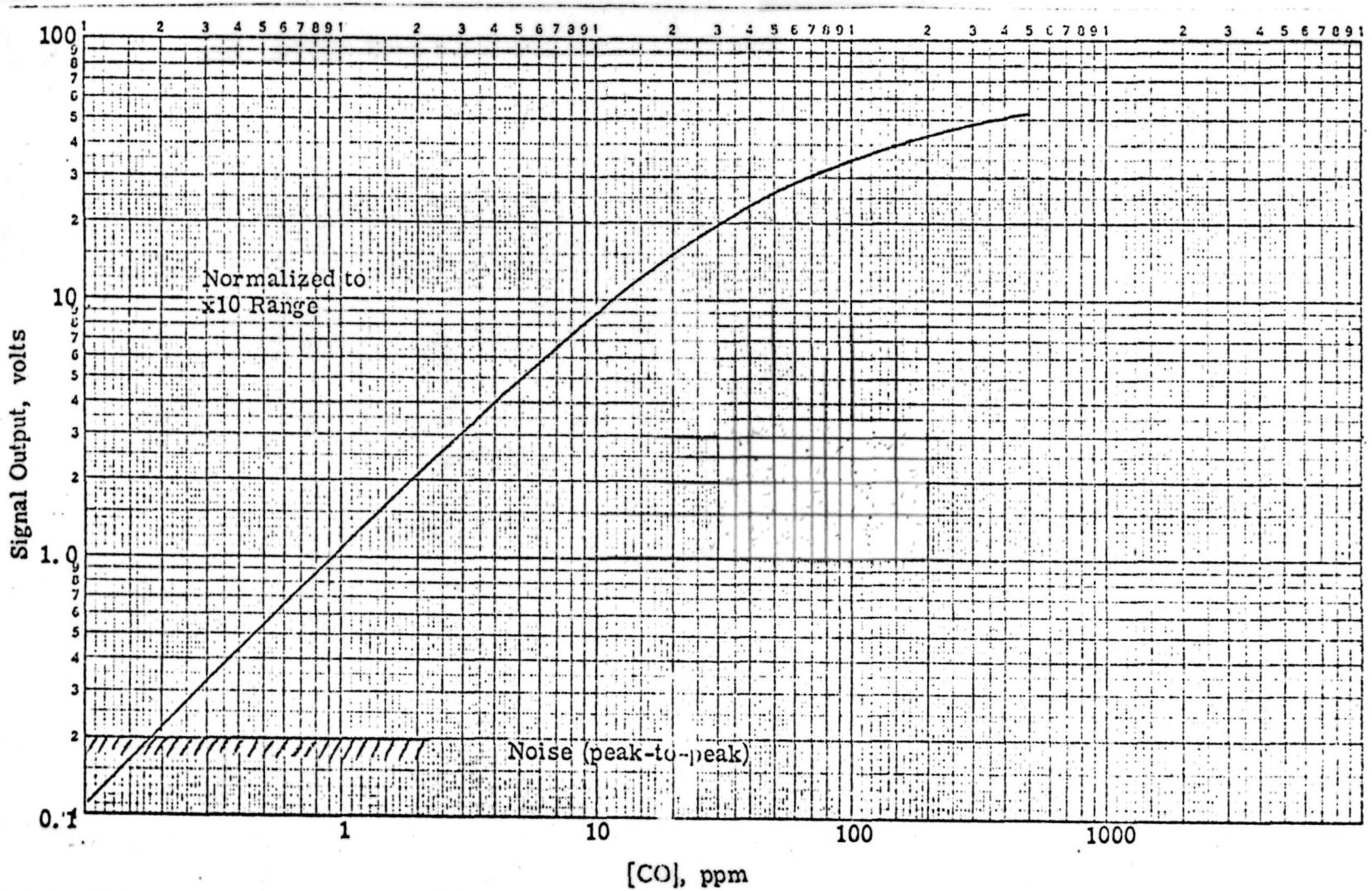

Figure 3-7. Output Response for 20 cm Optical Pathlength GFC Gas Analyzer to N_2 Diluted CO

As was done in Section 3.3.1, the theoretical and measured results may be compared. The results show that for 10 ppm CO a 10V signal should be obtained compared with the 9V signal observed. And, the calculated peak-to-peak noise is 125 mV compared with the 200 mV measured. This indicates a sensitivity of about 0.2 ppm CO.

3.4.2 Specificity

Measurements were made on the effects due to the presence of CO_2, N_2O, H_2O and HC1. The results are shown below.

Experiment	Results
CO + CO_2 + N_2O	350ppm CO_2 + 0.25ppm N_2O → <200ppb CO
CO + HC1	100ppm HC1 → no effect.
CO + H_2O	3.5% H_2O (=100% R.H. at 300K)→ -200ppb CO

Theoretical calculations for CO and interfering species are shown in Figures 3-8, 3-9 and 3-10. Again, comparing the theoretical and measured results, it appears that the theoretical calculations are overly pessimistic.

3.5 Corner Reflector Array (CRA)

The problem of an externally mounted IR beam reflector, located on the wing tip, is that of maintaining optical alignment when the wing flutters. This effect is overcome by using an array of small corner cube reflectors, since every ray is directly turned back on itself but, with a lateral displacement of up to the corner cube dimension. If the reflector is underfilled by the beam, an array of small corner cubes is therefore preferable to a single large corner cube retroreflector.

A triangular sub-array of 1cm first surface mirror corner cubes was developed. It is injection molded from a machined and polished master; it is then aluminized and overcoated with SiO. Using a number of sub-arrays, a single, large CRA may be assembled. This is illustrated by Figure 3-11.

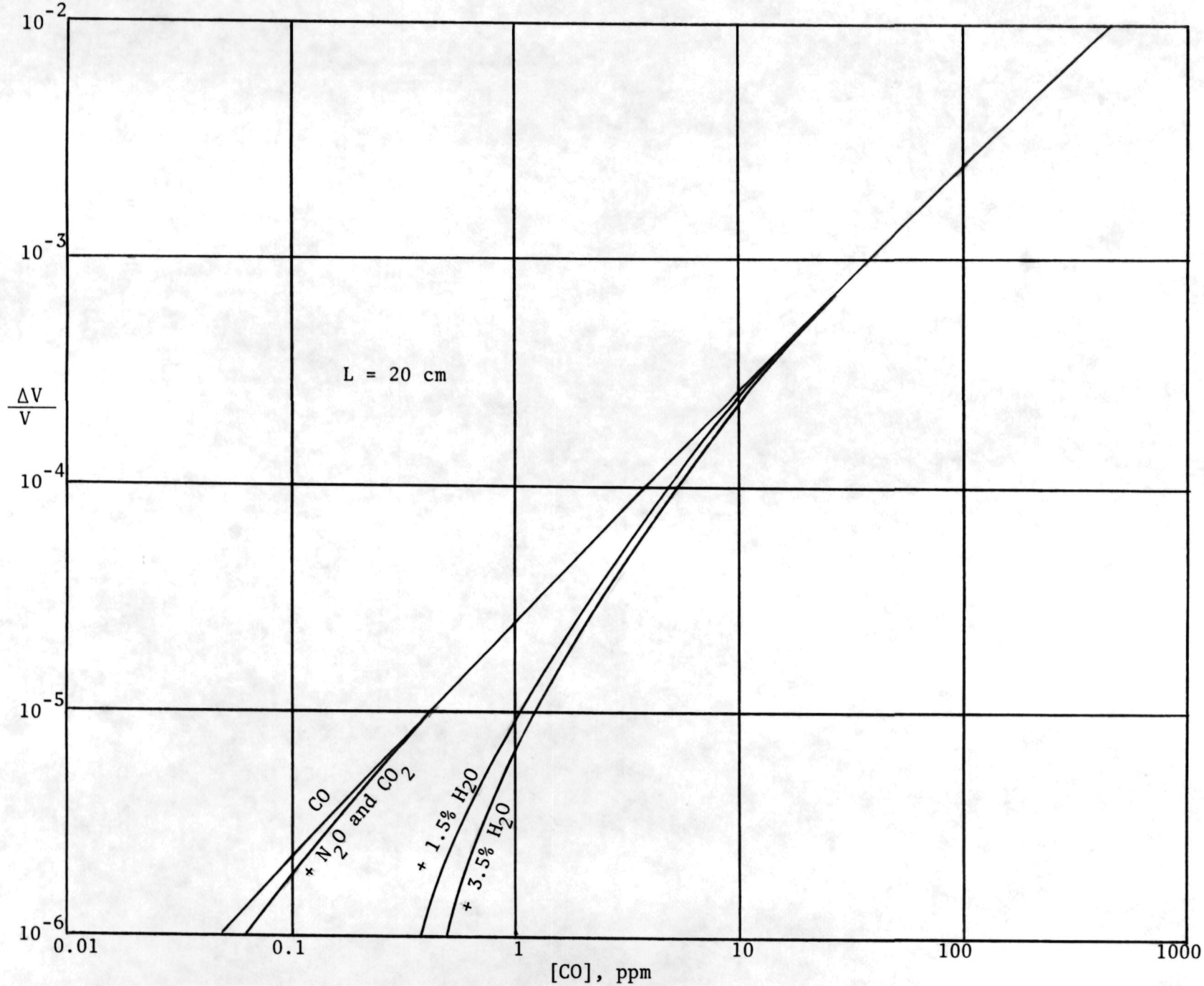

Figure 3-8. Theoretical Influence of Interfering Species on CO for L=20 cm

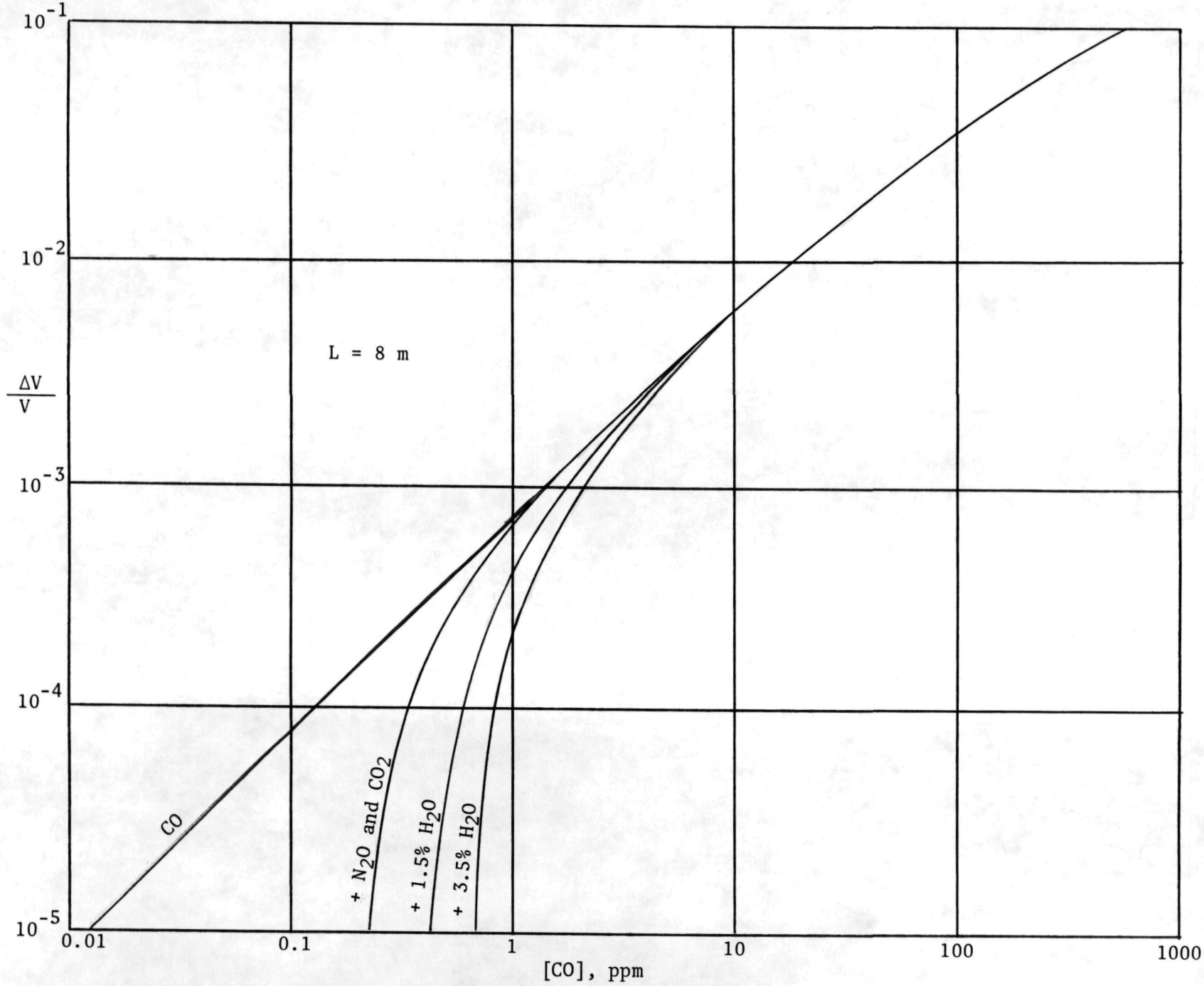

Figure 3-9. Theoretical Influence of Interesting Species on CO for L-8 m

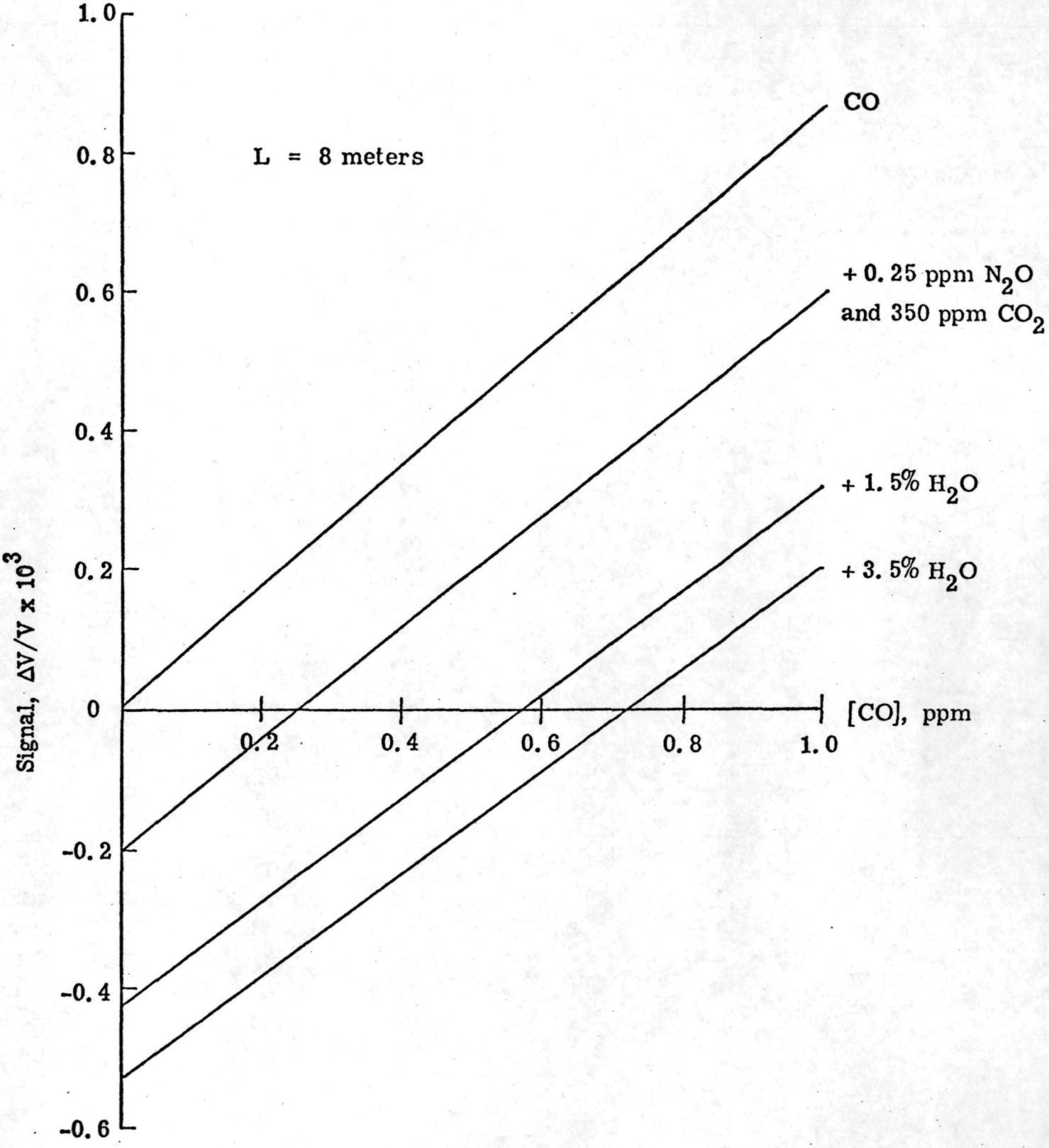

Figure 3-10. Theoretical Influence of Interfering Species on CO for L=8 m (linear plot).

Experiments were conducted using a single CRA unit, a He-Ne laser, beam splitter, auxiliary optics and a Silicon detector. The experimental set-up is shown in Figure 3-12. No change in signal level was observed by translational movement of 1cm or angular movement of 5 degrees of the CRA.

3.6 Summary and Conclusions

A GFC breadboard system was used to evaluate the technique for detecting HC1 and CO. The results indicate that adequate sensitivity can be obtained and that theoretical signal and noise equations can be used to design a flight system.

Specificity testing showed that the GFC technique will not be influenced by other species present in the exhaust cloud.

A corner reflector array was developed and tested. This array permits the mounting of a CRA on the wing tip that will be insensitive to wing motion, thereby eliminating optical alignment effects.

Although not mentioned, the testing of the breadboard did show two major drawbacks. One, the tuning fork choppers are vibration sensitive and not suitable for an aircraft instrument and, two, the split reference cell-specifying cell-reference cell configuration gives a serious drift problem due to changes in the near field-of-view and varying ambient temperature.

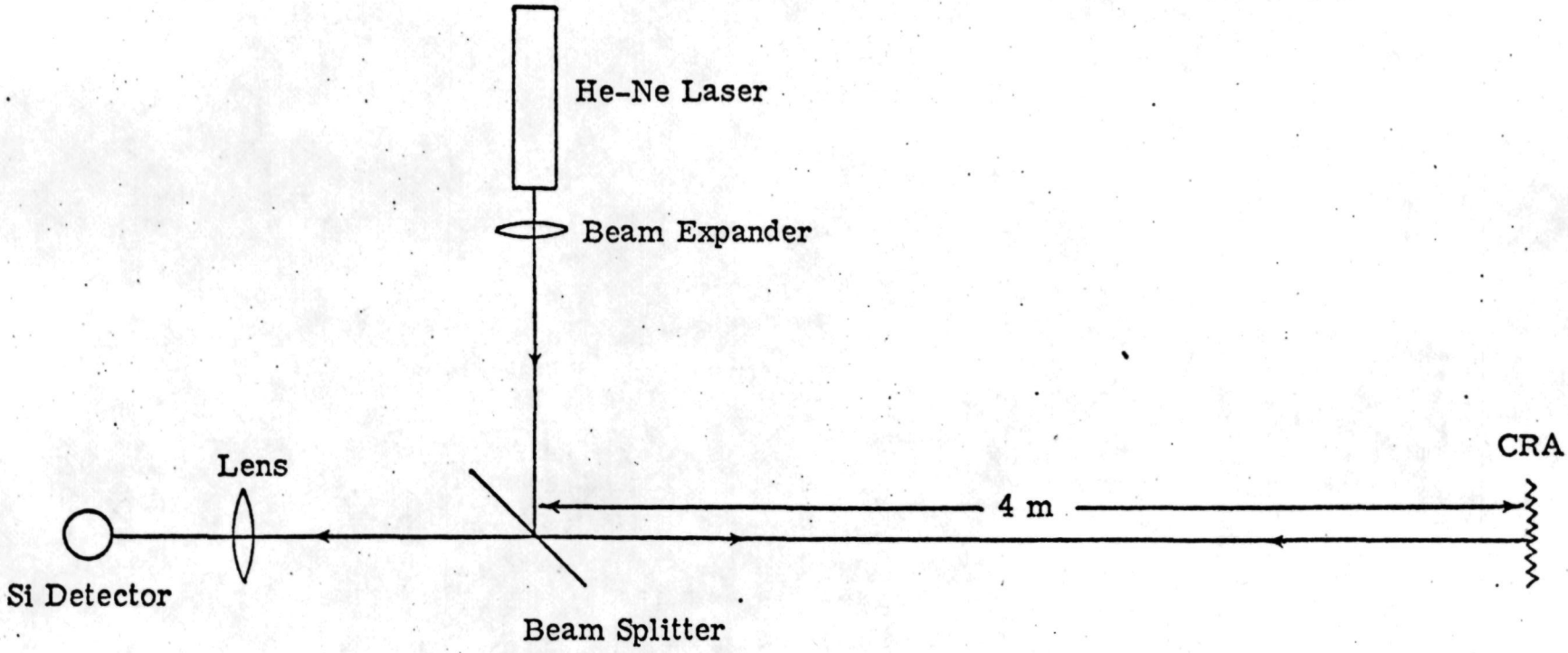

Figure 3-12. Experimental Set-Up Used to Evaluate CRA Unit

4.0 FLIGHT SYSTEM

Details of the system and its performance are documented in the Operation Manual. Thus, this section is abbreviated.

4.1 Optical-Mechanical System

The basic sensor is to be mounted inside the aircraft cabin. It directs an infrared beam of energy onto a Corner Reflector Array (CRA) that is to be mounted on the wing-tip fuel tank shrouding. The CRA re-directs the infrared energy, thus providing a measure of the mean concentrations of HC1 and CO between the sensor and CRA.

The optical-mechanical layout is shown in the scaled drawing (Figure 4-1). All components are shown to scale with respect to size and placement except the instrument window and the externally mounted CRA.

Figure 4-2 is a schematic of the chopping technique. The high temperature source radiance is chopped at 411 Hz by a multi-tooth blade which is coupled directly to the motor shaft. The beam is then modulated at 9.1 Hz by the low frequency rotation of the "split" cell. The "split" cell is coupled to the same motor through a 3:1 gear train to provide perfect synchronization of the two chopping frequencies.

The separate sections of the split cell contain HC1 and CO respectively. Since the spectral bands of the two gases do not overlap, the alternate cell is employed as a reference cell; e.g., HC1 in one cell is the specifying gas which absorbs at 3.4 μm while CO in the alternate cell does not absorb at this particular spectral interval, allowing this cell to be used as a reference cell for HC1. Both cells are filled with N_2-diluted gases to provide a mean transmissivity, τ_o, of 0.85 and hermetically sealed.

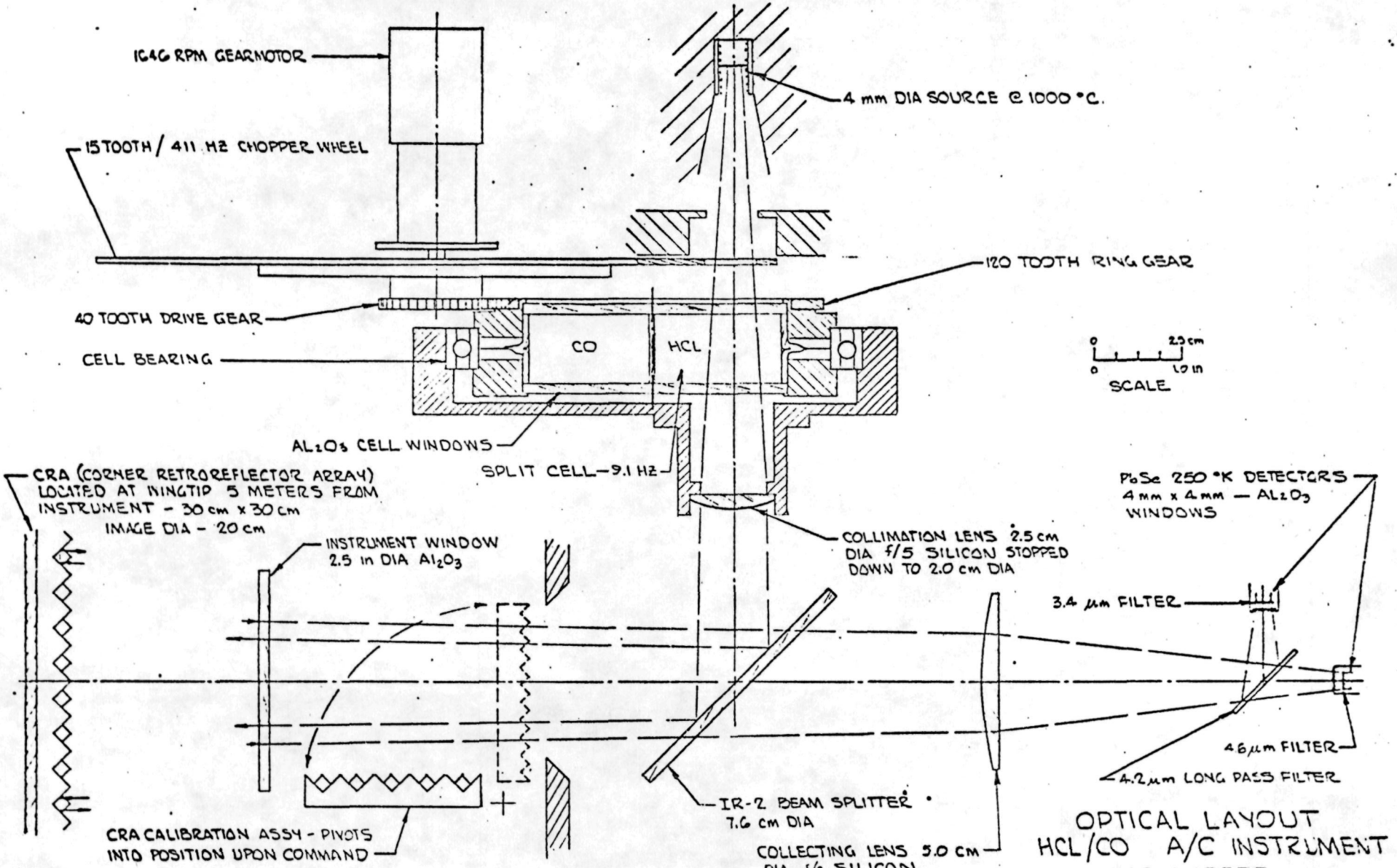

FIG. 4-1

OPTICAL LAYOUT
HCL/CO A/C INSTRUMENT
NAS 1-13573

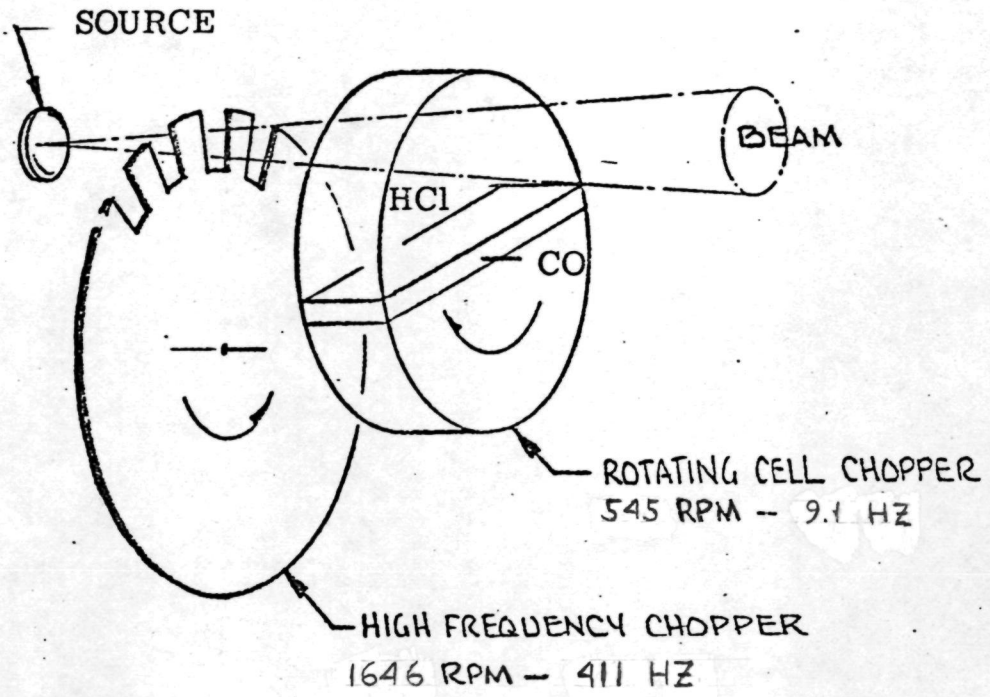

Figure 4-2. Schematic of Chopping Technique

The chopped source flux is collimated by an f/5 lens such that the beam dimension at the CRA located at 5m distance, on the wing tip, remains small (20 cm dia.).

A beam splitter directs the flux through the window which shields the instrument from the aircraft exterior environment to the CRA. The CRA reflects the beam back on itself. A fraction of the beam is transmitted by the beam splitter and brought to focus by the f/2 collecting lens.

A long pass filter reflects the 3.4 μm flux to a detector/filter combination for HC1 and transmits the 4.6 μm flux to the detector/filter combination for CO.

The detectors are both PbSe cooled to $-20^{o}C$ by two stage thermoelectric coolers; narrow pass band filters are included in each detector package (mounted in a TO-37 can). The specific detectivity at 411 Hz chopping frequency is conservatively estimated to be 5×10^{9} cm $Hz^{\frac{1}{2}}/W$.

The retroreflector (CRA) is a 30 x 30 cm array of 1 cm first surface mirror corner cubes. The total array is made up of mating triangular subarrays, each containing 60 corner cube reflectors. The property of a corner cube is that it returns a ray parallel to the incident ray, but with a lateral displacement of up to the corner cube dimension. An array of small elements therefore provides a smaller diameter return beam than would a larger reflector of the same accuracy. An additional benefit is that a large array can be assembled, which is thin, lightweight, and can be inexpensively and quickly repaired, if necessary. Because a corner cube is insensitive to alignment, a heavy rigid support structure is not needed and a lightweight assembly is provided.

The arrays are injection molded from a machined and polished master; the arrays are then aluminized and overcoated with SiO. The specified accuracy of the reflector elements is that they return a beam with a angular deviation of 6 arc minutes or less with respect to the incident beam.

4.2 Electronics

As discussed in the description of the optical layout, the HC1 and the CO measurements use a common source, chopper and optical system, but are imaged onto separate detectors by the 45^{o} filter. This permits the use of separate, identical signal processing circuits with common circuits for the generation of the synchronous demodulation pulses, chopper drive and power supplies.

A block diagram of the electronic system is shown in Figure 4-3.

A signal processing sequence begins at the detector. For each gas, the detector is a photoconductive PbSe device on a two-stage thermo-electric cooler. The TE cooler power supply is a controlled current circuit using the detector resistance as the sensor to ensure a stable detector temperature. The detector bias voltage is obtained from a very well filtered regulated supply. The heavy filtering is required because noise on the bias directly degrades the signal/noise ratio and is practical because of the very low current required.

The signal output of the detector is a 411 Hz "carrier" amplitude modulated at 9.1 Hz by the rotating gas cell. The amplitude of the 411 Hz signal is the V signal (proportional to source radiance) and the amplitude of the 9.1 Hz modulation contains the ΔV (pollutant) term as well as an imbalance term which is removed after the first demodulator. In addition to the 411 Hz, a small component may be present at 9.1 Hz, but only the 411 Hz component is accepted by the first demodulator.

A preamp is located immediately adjacent to each detector. This serves to increase the signal to such a level that subsequent noise introduction will not degrade the S/N ratio. It is expected that the preamp will not contribute appreciable noise because of the relatively high noise output inherent to PbSe detectors.

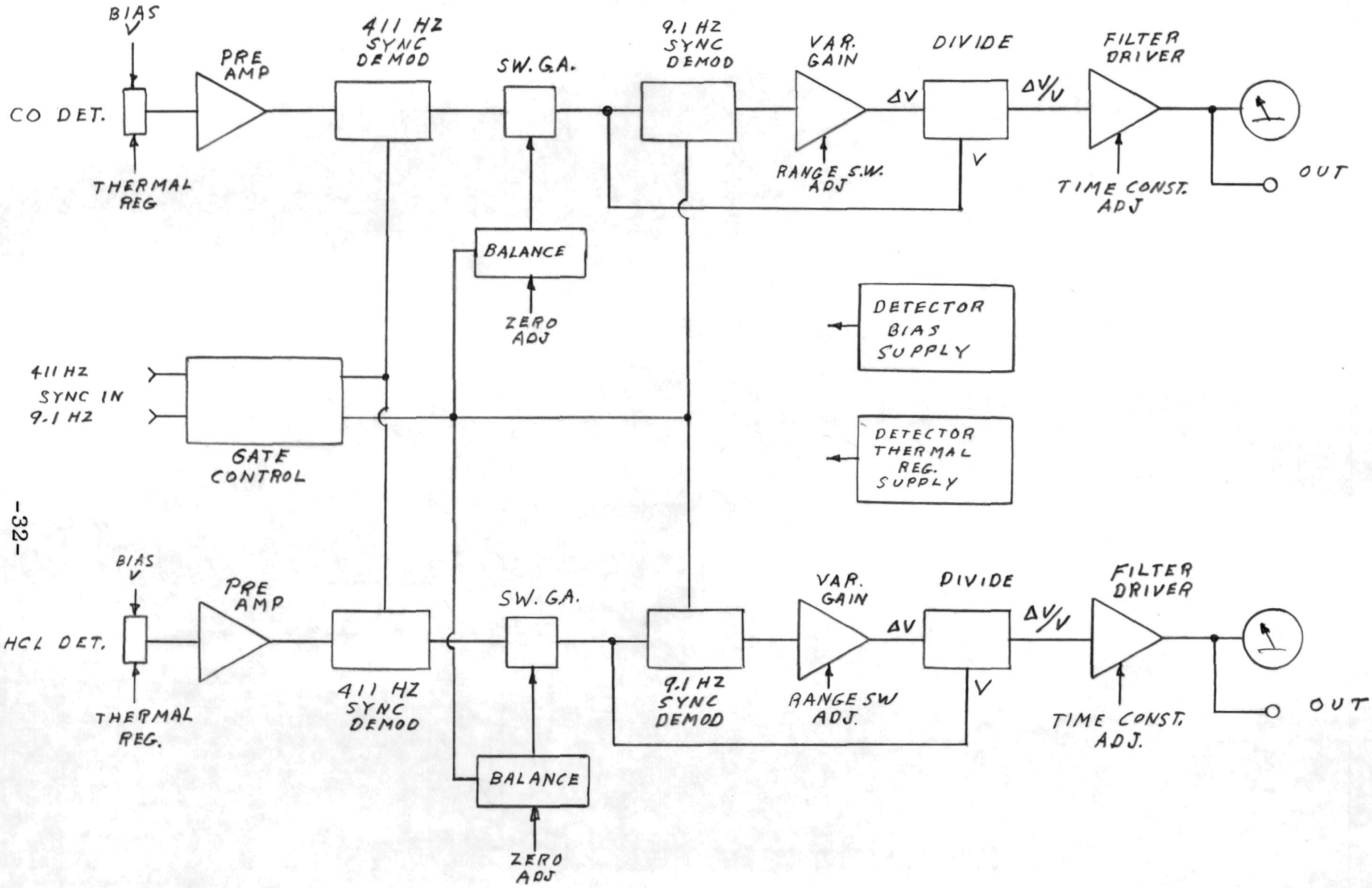

Figure 4-3. Electronics Block Diagram

The first synchronous demodulator consists of two sample-hold modules and a summing amplifier and operates with gate pulses derived from the 411 Hz wheel chopper. The output is a DC voltage equal to the 411 Hz carrier amplitude and a superimposed 9.1 Hz square wave ripple equal to the carrier modulation. Any signals at other than 411 Hz will not pass this synchronous demodulator.

Next, the balance correction is introduced. The condition to be satisfied is that zero ΔV signal (= zero amplitude modulation) exist for zero pollutant gas concentration in the optical path. The physical condition to satisfy this would be that the total source energy passing through the specifying cell be equal to that through the reference cell. However, in this two gas design in which each cell serves both as the specifying cell (for one gas) and as the reference cell (for the other gas), it is not possible to simultaneously balance both gas systems by aperture adjustment. Consequently, an electronic analog of aperture balancing is employed. To accomplish this the signal out of the first synchronous demodulator is amplified by a stage having its gain switched in phase with the 9.1 Hz signal; the gains being of such amplitudes that the 9.1 Hz signal is reduced to zero. This serves as a "zero" adjustment. Moving the CAL/DATA switch to CAL moves a cover containing a small retroreflector into the near field-of-view. There is thus no pollutant gas in the optical path and the output can be nulled for each gas individually using the ZERO controls on the instrument panel. Electronically, this is accomplished by adjusting the relative gains of the switched gain stage.

The "span" adjustment operates on a similar principle. Placing the SPAN/DATA switch to SPAN introduces a known change in the amplitude of the balance square wave. This causes a shift in the output data which is proportional to the overall

sensitivity and corresponds to a calibrated scale output. The SPAN panel adjustment varies the electronic gain to set the output signal to the prescribed value.

The DATA position of the CAL/DATA switch opens the entrance aperture to the external retroreflector.

The remainder of the signal processing system is straightforward. As previously explained, the amplitude of the 411 HZ carrier is the V signal; the amplitude of the 9.1 Hz modulation is the ΔV signal.

The second synchronous demodulator also consists of two samplehold modules and a summing amplifier and operates at 9.1 Hz. The output is the ΔV signal; the span and range variable gain stage operates on this signal. Range selection in steps of 1, 10, 50 and 500 are provided.

At this point the ΔV and V signals exist separately and are ratioed in a divider module to eliminate the source term from the modulation function.

A low-pass filter is provided with a variable (two-position panel - switched) time constant so that low level signals can be read to a higher precision when conditions permit the longer integration time. The two time constants are 0.5 and 10 seconds.

A driver stage provides a low impedance output to the panel meters and recorder jacks.

A photograph of the front panel of the sensor is presented in Figure 4-4.

4.3 Design Performance

Following the presentation in Section 3.2, the values of the flight instrument parameters are presented in Table 2. The theoretical detectable limits for $S/N_{p-p}=1$, using a 10 second time constant, are calculated to be 99.5 and 70.0 ppb for HC1 and CO, respectively.

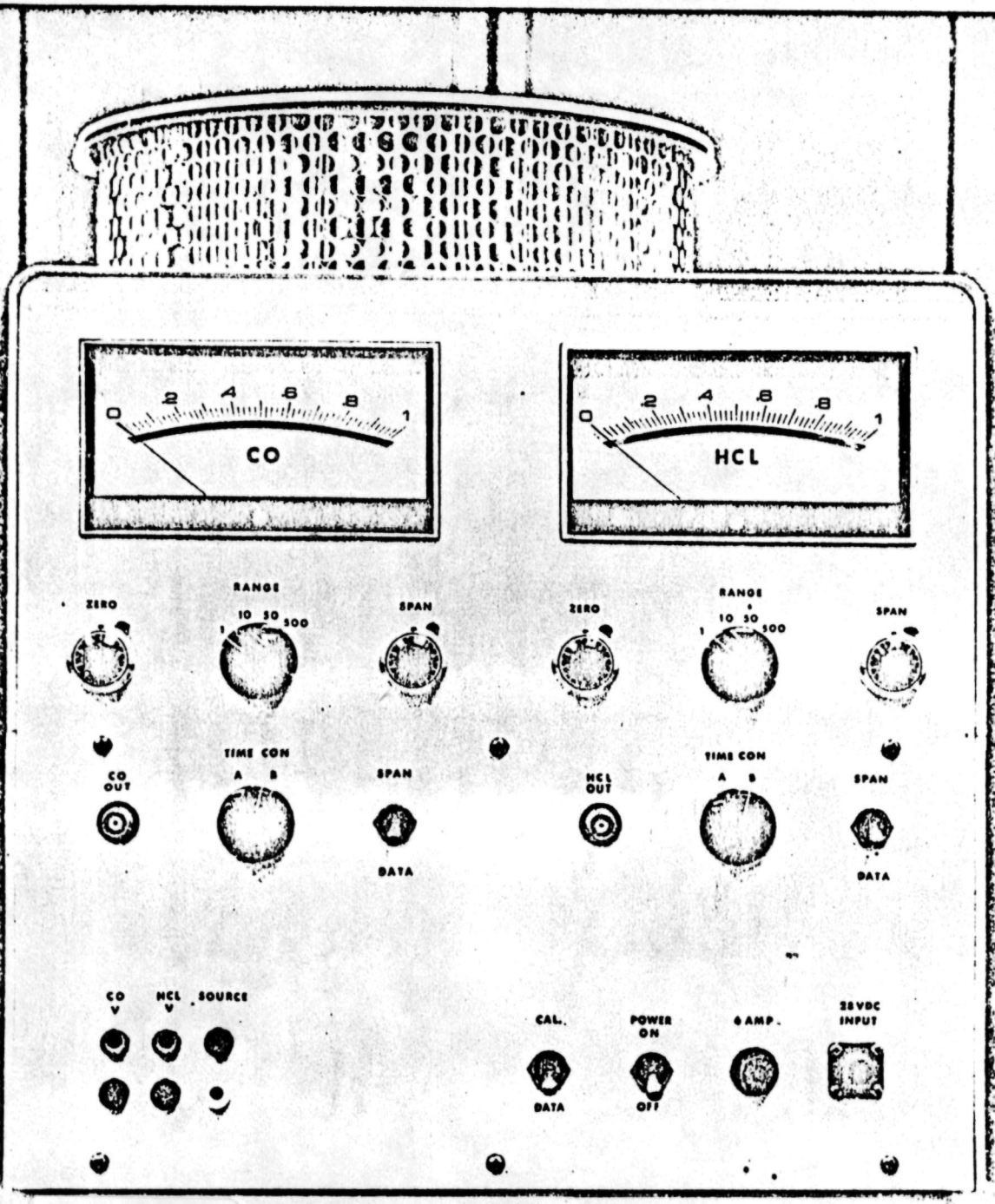

Figure 4-4. Photograph of control panel of the sensor.

TABLE 2. SUMMARY OF FLIGHT INSTRUMENT PARAMETERS

Parameter	HCl	CO	Note
η	8×10^{-3}	8×10^{-3}	a
A, cm^2, source lens	3.1	3.1	
Ω, sr	7.8×10^{-4}	7.8×10^{-4}	b
$N^o(T = 1000^oC) W/cm^2-\mu-sr$	0.47	0.26	
τ_o	0.85	0.85	
$\bar{k}$, atm^{-1} cm^{-1}	0.5	1.5	
L, cm	10^3	10^3	c
P, atm	1.0	1.0	
$\Delta\lambda$, μm	0.14	0.12	
R, V/W	8.9×10^3	8.9×10^3	
A_d, cm^2	0.16	0.16	
Δf, Hz	0.075	0.075	d
D*, cm $Hz^{\frac{1}{2}}/W$	10^{10}	10^{10}	e
S(C=11), V	4.88	6.94	
N_{rms}, V	9.75×10^{-8}	9.75×10^{-8}	
C_{min}	19.9 ppb	14.0 ppb	f

[a] $$\eta = (\tau_w)^2(\tau_{sl})(\rho_{bs})(\tau_w)^2(\eta_{cra})(\tau_{bs})(\tau_{dl})(\eta_f)(\tau_f)(\eta_e) \quad (4\text{-}1)$$

$$= (.88)^2(.95)(.32)(.88)^2(.23)(.68)(.95)(.7)(.7)(.8)(.75) = 8 \times 10^{-3}$$

[b] solid angle subtended by source, seen from source lens

[c] assumes 10m optical path (double pass; 5 m each way)

[d] for a 10 second time constant

[e] nominal manufacturer's value at $\tau_d = -30^oC$

[f] for $S/N_{rms} = 1$

4.4 Laboratory Test Results

Measurements of the signal and noise for both HC1 and CO were made by inserting N_2-diluted test gas mixtures in a 50 cm long cell with 7.62 cm dia sapphire windows. The sensitivity results are shown in Figures 4-5 and 4-6 in terms of the optical thickness in ppm-m normalized to the 0-1 ppm range.

The final peak-to-peak noise measurements gave the following Noise-Equivalent-Concentrations for a 10 m optical path.*

Species	Time Constant	NEC,ppm
HC1	A = 0.5 sec	2.0
HC1	B = 9 sec	0.45
CO	A = 0.5 sec	1.0
CO	B = 9 sec	0.23

Comparing these data with calculated sensitivities show that actual performance is about five times worse than anticipated. However, no actual data was provided by the detector manufacturer for specific detectivity and, the D* ($=10^{10}$) used for the calculation may have been overly optimistic.

* Revised values, see Appendix B "System Noise."

Figure 4-5.

HCl Calibration, Normalized to x1 Range

Span = 73% Full Scale on x50 Range

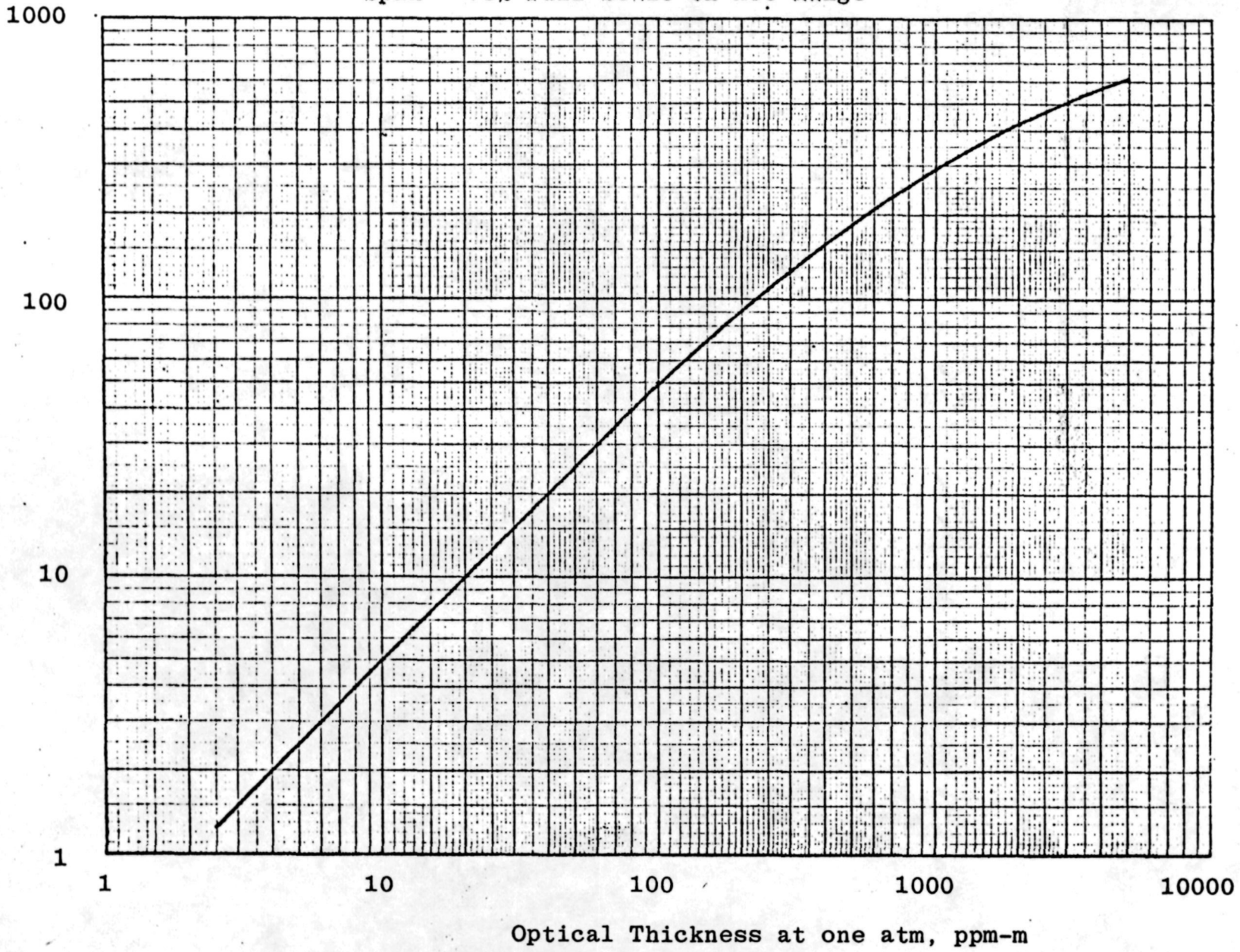

Figure 4-6.

CO Calibration, Normalized to x1 Range
Span = 70% Full Scale on x50 Range

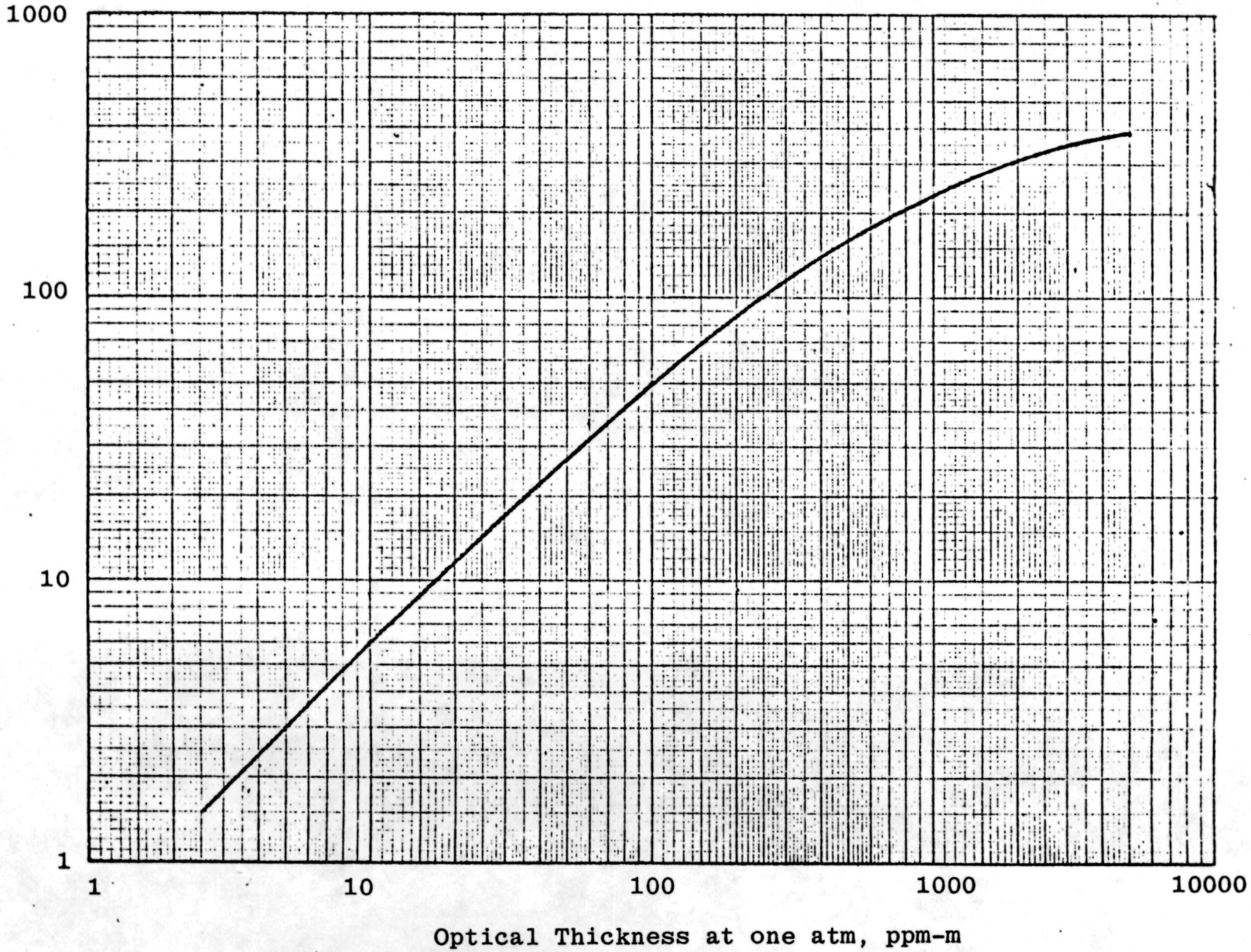

5.0 FLIGHT TESTS

5.1 Installation and Preliminary Test Flights

After shipment of the system to NASA, it was re-tested by NASA personnel. It was discovered that both the HC1 and CO channels had become noisier than the data shown in Section 4, by about a factor of 5. Calibration checks showed excellent agreement with the HC1 calibration (Figure 4-5) but, the CO calibration data at NASA indicated signals about 25 percent lower than those shown in Figure 4-6.

The system was installed in the chartered Cessna 402 aircraft. Figures 5-1, 5-2 and 5-3* illustrate the installation.

Figure 5-1 shows the mounting of the sensor in the aircraft together with the other instruments aboard and the PADS data acquisition system.

Figure 5-2 shows an overview of the aircraft with the sensor view port and the back of the CRA.

Figure 5-3 shows a front view of the mounted CRA.

---

* Note - NASA LRC has glossy prints of these photographs.

Figure 5-1. HC1-CO Sensor Installation in Cessna 402.

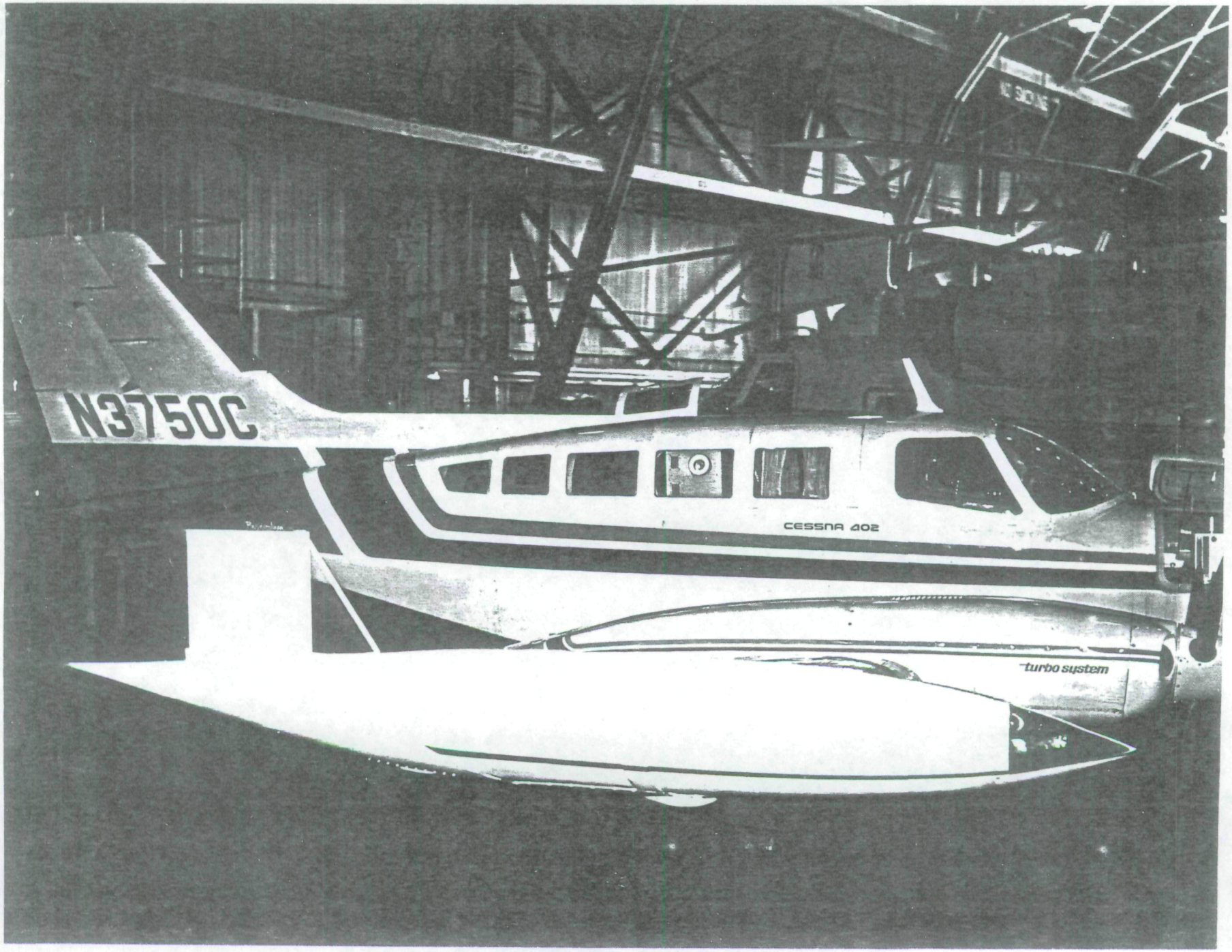

Figure 5-2. Sensor Viewing Port and Wingtip Retroreflector.

Figure 5-3. Retroreflector Installation of Wingtip Pod Shroud.

After installation of the system, the sensor-retro-reflector separation was measured as 5.36 meters, giving a total optical path of 10.72 meters. Using this value, the calibration data has been established for the X 50 ranges. The results are shown in Figures 5-4 and 5-5.

A 2 3/4 hour test flight was conducted and several important results obtained.

1. The sensor did not have to be re-aligned during flight conditions.
2. The "noise" levels during flight were the same as on the ground.
3. No effects were observed by turning off the engine between the sensor and retroreflector.
4. No radio interferences were observed.
5. The sensor zero and span levels remained stable throughout the flight.
6. Some degradation in V signal was noted. This is believed to be caused by a gradual warming of the detectors.
7. A pass over the Yorktown refinery indicated an increase in CO of about 2 ppm.
8. A pass over the West Point pulp mill indicated an increase in CO of about 5 ppm.

Figure 5-4

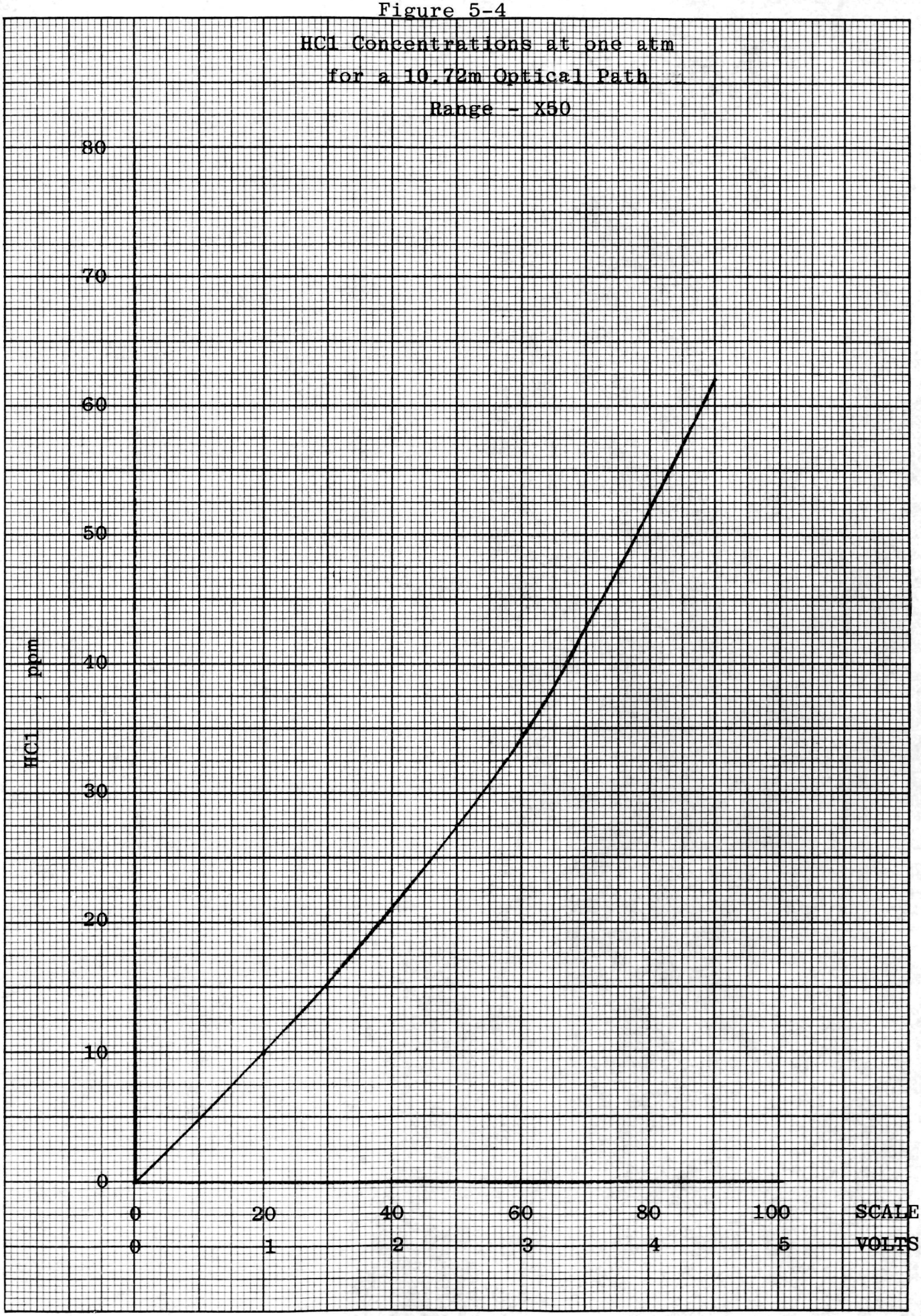

Figure 5-5

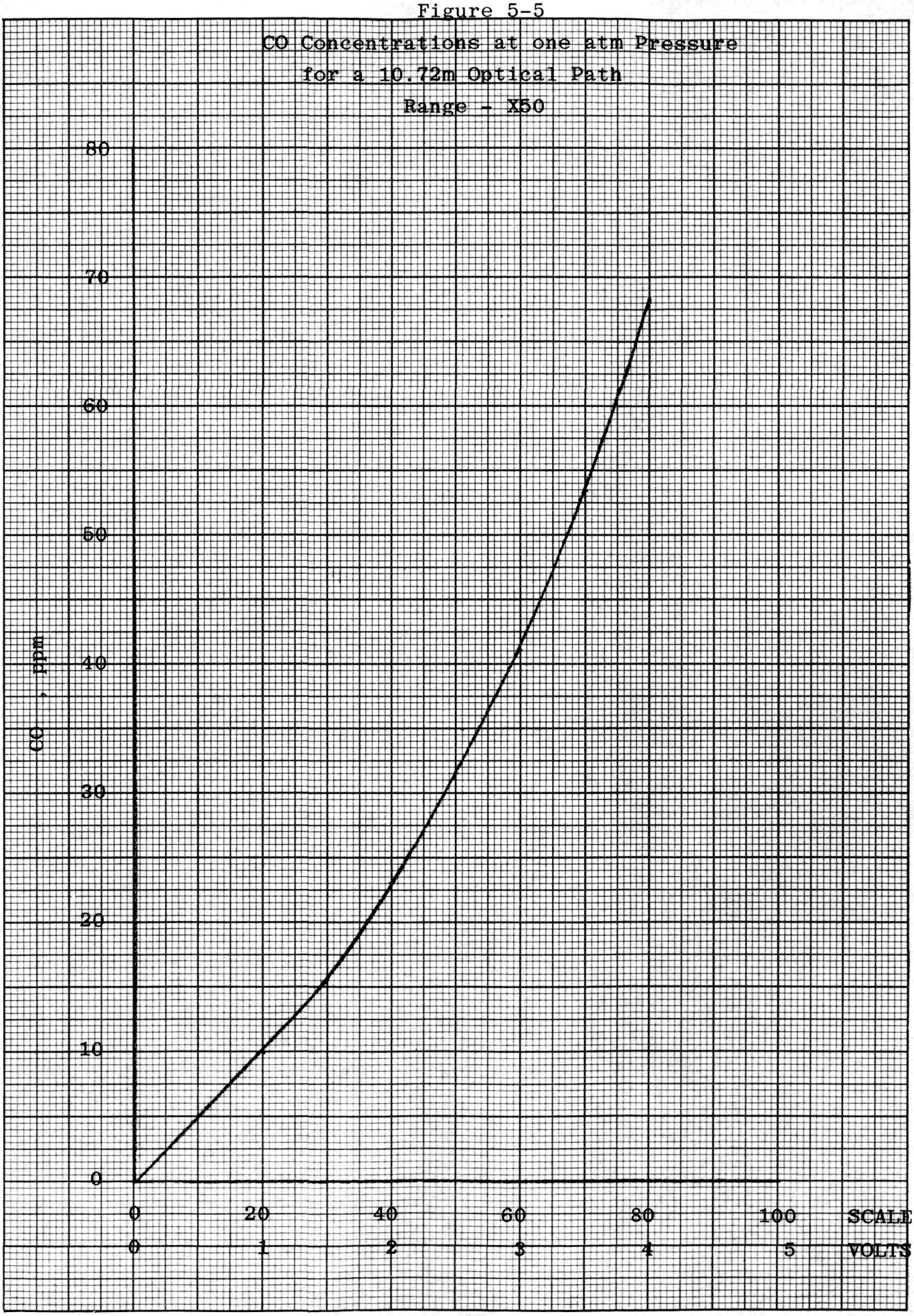

5.2 Mission Test Flight

The GFC sensing system was flown through an actual rocket exhaust cloud. The cloud was generated by a Titan 3C rock launched from Kennedy Space Center at 20:25 EDT on March 14, 1976.

Both the HC1 and CO channels functioned throughout the flight.

Prior to the actucal mission:

1. The retroreflector was re-installed on the aircraft.
2. The sensor system was tested; no shift in zero or span settings had occurred from the time the system was initially test flown from LaRC.
3. A test flight made from PAFB through a natural cloud indicated that extreme turbulence could cause a significant optical mis-alignment and invalidate the data.
4. As a result of (3) the vibration mounts were removed and the sensor was bolted directly to the equipment shelf. Photograph Figure 5-1 was taken with the original mount configuration. This appeared to eliminate the turbulence problem as determined by severely rocking and wing tip on which the retro-reflector was mounted.
5. No shift in zero or span was observed even though the system was operated in the aircraft over temperature ranges from $10^{o}C$ to $38^{o}C$ ($50^{o}F$ to $100^{o}F$).

Following the mission flight, the recorded data was examined. Figure 5-6 is a tracing of the flight recording of the CO and HC1 data during the first pass. An unexpected phenomena is apparent that invalidates most of the data. Namely, that most of the data indicates a negative correlation between the HC1 and CO channels; when one channel given a large positive signal, the other channel gives a large negative signal. The negative excursions are not seen in Figure 5-6 because the output

of the instrument is clipped at zero volts. However, there are a number of instances where the CO channel remained positive and a simultaneous positive response was observed from the HC1 channel. An example is seen in Figure 5-6, pass #1 flight data, where at 21.5 seconds the HCl reads 16 ppm above its zero offset.

At such times when this negative-correlation effect did not exist, peak concentration data that are believed valid were obtained. These are summarized below:

Pass	HC1, ppm	Time (launch:20:24 EDT)
1	16	20:30:21.5
6	16	20:42:04.5
6	7	20:42:35
7	6	20:44:03
7	5	20:44:13
8	12	20:49:48
8	6	20:50:01
8	8	20:50:06
9	8	20:52:08.5
10	6	20:54:12
10	8	20:54:15
14	5	02:02:02
14	8	02:02:39
15	3	02:04:29
18	2	02:11:50
18	3	02:12:08
18	3	02:12:19
20	5	02:16:47

No CO was observed above the noise level - 1 ppm.

Figure 5-6
Flight Data, Pass No. 1

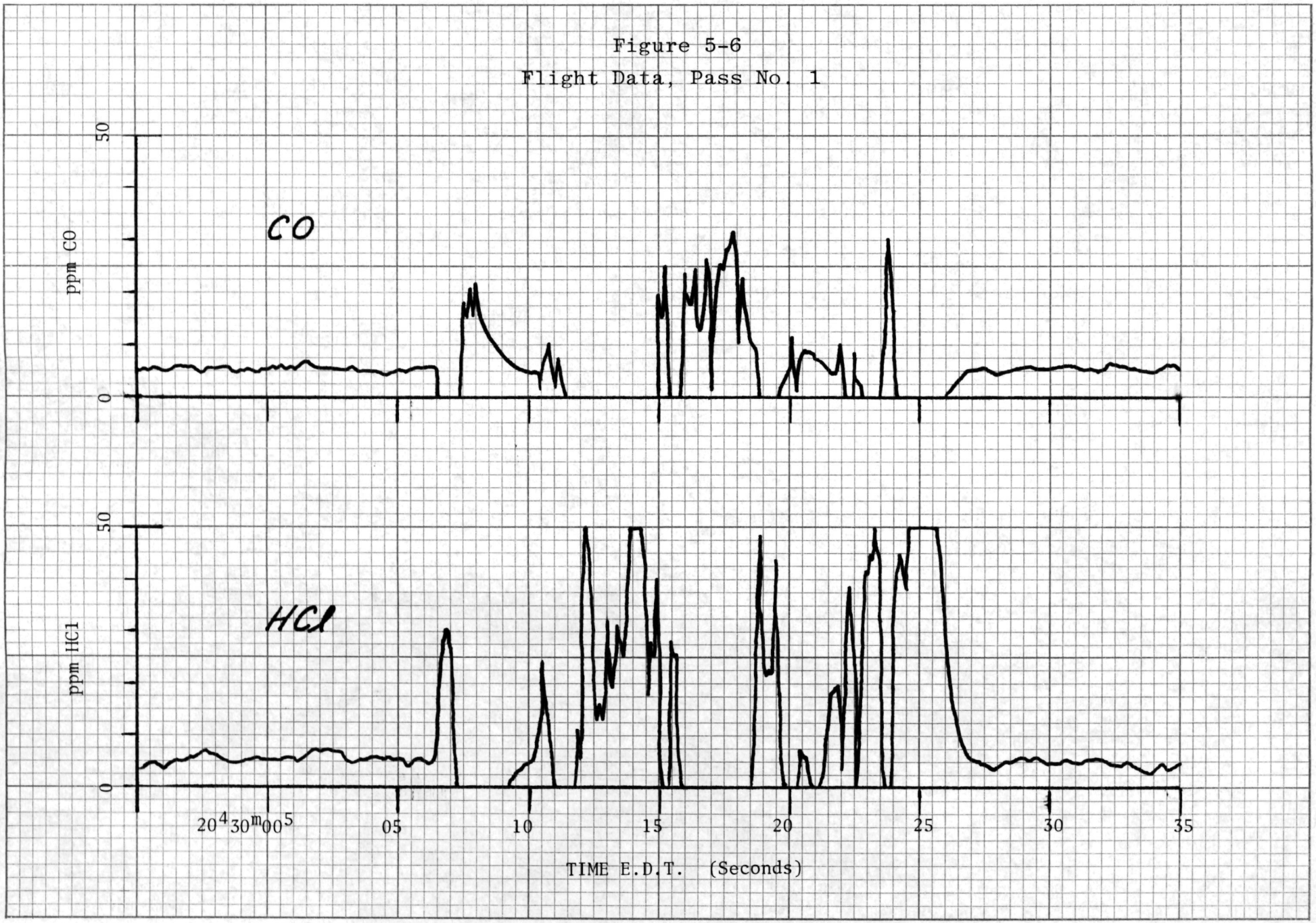

6.0 DISCUSSION

The GFC sensor system has proven to be a viable technique for measuring gaseous pollutants, in-situ, using an aircraft. Besides the present application of measuring HCl and CO in rocket exhaust plumes, many other applications are possible; such as measuring local urban pollutants, regional air pollutants, and even stratospheric pollution.

However, the operational field program revealed several problems in the delivered system.

1. Upon receipt of the instrument at NASA-LaRC, the noise levels on the CO and HCl data outputs were approximately a factor of five times higher than stated by SAI before shipment. The calibration curves for the CO and HCl had not changed. The high noise level remained through the mission flight.
2. The large amplitude negative correlation phenomenon between the CO and HCl data during the mission flight was not seen at SAI, nor did it occur during the test flight at PAFB.
3. A data output zero offset exists which is a function of the distance to the retroreflector. As a consequence, there is a zero offset between data taken with the internal calibration retroreflector and the aircraft wingtip retroreflector.

Following the completion of the operational mission flight, the instrument was returned to SAI, at SAI's request, for investigation of these problems. The results of this investigation are included as Appendix B to this report.

REFERENCES

1. C. B. Ludwig, et al, "Study of Air Pollutant Detection by Remote Sensors", NASA CR-1380, July 1969.

2. C. B. Ludwig, et al, "Air Pollution Measurements from Satellites", NASA CR-2324, November 1973.

3. Bartle, E. R. et al, "An In-Situ Monitor for HC1 and HF", AIAA Paper No. 71-1049, November 1971; J. Spacecraft and Rockets, 11, 836, 1972.

4. Ludwig, C. B. et al, "Remote Measurement of Air Pollution by Nondispersive Optical Correlation", AIAA Paper No. 71-1107, November 1971; AIAA Jr. 11, 899, 1973.

5. Bartle, E. R. "Infrared Sensor for the Remote Monitoring of SO_2" EPA-650/2-75-041, May 1975.

6. Bartle, E. R., "A Portable Gas-Filter-Correlation Spectrometer for HC1 and HF", USAF SAM-TR-75-33, October 1975.

7. H. F. Luft, Z. Techn. Phys. 24, 97 (1943).

8. A. H. Pfund, Sci. 90, 326 (1939); Bull. Johns Hopk. Hos. 67, 61 (1940).

9. H. Schmick, U.S. Patent No. 1, 758, 088.

10. N. Wright, L. W. Herscher, JOSA 36, 195 (1946).

APPENDIX A

THEORY OF OPERATION

Infrared absorption spectroscopy has long served as a powerful technique for gas mixture analysis. In contrast to dispersive spectroscopy, a nondispersive infrared (NDIR) device makes use of the particular gas to provide specificity.

Refinements of NDIR have been made recently through a better understanding of the monochromatic spectroscopic properties of gases.

If the optical thickness of the comparison gas in the sensor is kept small, an ultimate high-spectral-resolution filter (provided by the natural line-width of the gas) results. High spectral resolution is the most important parameter in obtaining specificity and accuracy in pollutant analysis. The term "gas filter correlation" (GFC) was adopted to describe the sensors using this technique.

GFC is based upon absorption or emission of electromagnetic energy by the specific pollutant to be monitored. As such, GFC can operate in the UV, visible, or IR regions of the spectrum. The IR may be preferable because <u>all</u> pollutants of interest have rotational lines that absorb in the IR; also, scattering effects are more pronounced in the UV and visible. On the other hand, the UV-visible may be preferable if extreme spectral interferences occur in the IR; also, more sensitive photo-multiplier detectors are available and pollutant absorptivities are greater.

Conventional spectroscopic instruments depend upon finding a <u>single</u> absorption line of a particular species. GFC uses the contribution of <u>all</u> absorption lines of a particular species' band system.

Specificity is obtained by using random correlation between spectra arising from the particular and the interfering species; the principle of random correlation has been established for most pollutant species and for interfering species occurring naturally and in polluted atmospheres. In addition, a ratioing technique may be used that minimizes effects of source intensity changes, background radiation, and continuum absorption due to complex molecules, aerosols, or water vapor.

GFC technique can be applied to both double-and single-ended systems. For the double-ended system, an active infrared source and GFC receiver are used to measure an intervening pollutant; in this case, the detection principle is based upon absorption spectroscopy. For the single-ended system, only the GFC receiver is used to remotely detect a pollutant; in this case, the detection principle is based upon either emission or absorption spectroscopy, depending upon the relative temperatures of the pollutant to be detected and the background.

A schematic diagram which illustrates the apparatus used for initial laboratory studies is presented in Figure A-1. The basic components are a high-temperature infrared source; a sample cell in which the gas mixture to be analyzed is placed; a rotating chopper; a reference cell containing a vacuum or a transparent gas such as nitrogen; a specifying cell containing a sample of the gas to be detected; an adjustable aperture limiting the radiation passing through the reference cell; an optical filter confining the radiation to the spectral region where the gas to be detected possesses absorption bands; a sensitive infrared detector; and optics to collimate the radiance from the source and to focus it on the detector. The radiation from the source passes through the sample cell where it is spectrally absorbed by the specific gas and possible interfering gases. The radiation, having traversed the sample cell, is alternately passed through the reference and specifying cells. When passing through the reference cell, the radiation

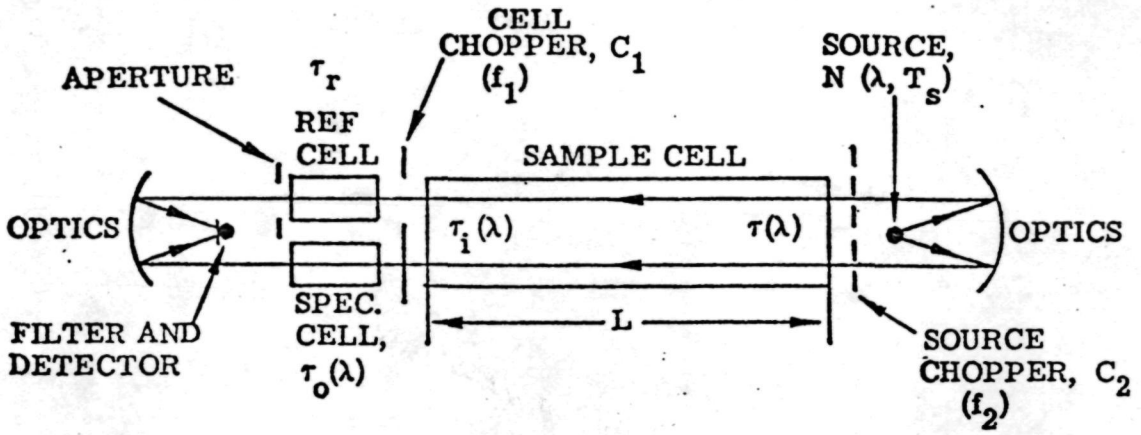

Figure A-1. Schematic diagram of double-ended GFC technique.

is unattenuated; but when passing through the specifying cell, it is attenuated by the spectral absorption character of the gas in the cell. Thus, an alternating signal is generated at the detector. The magnitude of this signal is related to the concentration of the gas to be detected in the sample cell.

The following development assumes that self-emission by the sample gas is negligible compared with the source radiance, N. Referring to Figure A-1, when the cell chopper at frequency f_1 is in the position indicated, the energy from the source which reaches the detector through the reference cell is given by

$$E_1 = \int_{\Delta\lambda} C(\lambda) N(\lambda, T_s) \tau_i(\lambda) \tau(\lambda) \tau_r d\lambda \qquad (1)$$

where

$C(\lambda)$	is the spectral attenuation due to the optics, cell windows, and optical filter;
$N(\lambda, T_s)$	is the radiance from the source;
$\tau_i(\lambda)$	is the spectral transmission through possible interfering gases;
$\tau(\lambda)$	is the spectral transmission due to the gas to be detected;
τ_r	is the transmission through the aperture.

E is obtained by integrating over the spectral wavelength interval $\Delta\lambda$ defined by the optical filter. Radiation, due to self-emission by the gases, windows, and other instrument components, is neglected, since for source temperatures greater than 1000°K and wavelengths less than 5 μm, the radiance from the source is at least three orders of magnitude greater than the radiance from 300°K materials.

Similarly, when the cell chopper passes radiation through the specifying cell, the energy reaching the detector is given by

$$E_2 = \int_{\Delta\lambda} C'(\lambda) N(\lambda, T) \tau_i(\lambda) \tau(\lambda) \tau_o(\lambda) d\lambda \qquad (2)$$

where $\tau_o(\lambda)$ is the transmission due to the gas in the specifying cell and $C'(\lambda)$ is the spectral attenuation due to the optics.

The peak-to-peak signal difference at the detector by chopping is proportional to the difference between E_2 and E_1; that is,

$$\Delta V \alpha E_2 - E_1 = \int_{\Delta\lambda} N(\lambda, T) \tau_i(\lambda) \tau(\lambda) \left[C'(\lambda) \tau_o(\lambda) - C(\lambda) \tau_r \right] d\lambda \qquad (3)$$

Now, for slowing varying functions in λ, $N(\lambda, T_s)$ and $C'(\lambda)$ can be averaged over the interval $\Delta\lambda$. Thus,

$$\Delta V \alpha \bar{N} \bar{C}' \int_{\Delta\lambda} \tau_i(\lambda) \tau(\lambda) \left[\tau_o(\lambda) - \frac{C(\lambda)}{C'(\lambda)} \tau_r \right] d\lambda \qquad (4)$$

where the bars indicate mean values over $\Delta\lambda$. But, $\tau_o(\lambda)$ and $\tau(\lambda)$ are strongly correlated, since they represent the spectral transmission due to the same gas, and $\tau_i(\lambda)$ is assumed to be uncorrelated with $\tau_o(\lambda)$. Then, applying the mean value theorem,

$$\Delta V \alpha \bar{N} \bar{C}' \bar{\tau}_i \left[\overline{\tau \tau_o} - \overline{(C/C')} \bar{\tau} \tau_r \right] \Delta\lambda \qquad (5)$$

Since the two parameters $C(\lambda)$ and $C'(\lambda)$ differ from each other by only very minor differences between the nominally identical optical paths, the product of their ratio and the instrument adjustable aperture transmission may be considered to be an effective aperture, τ_r'. Thus,

$$\Delta V = K \bar{N} \bar{\tau}_i \left[\overline{\tau \tau_o} - \bar{\tau} \tau_r' \right] \tag{6}$$

for a given set of instrument parameters, where K is a proportionality constant.

To zero the instrument, the optical path is made transparent ($\tau = \tau_i = 1$) and the aperture adjusted such that $\tau_r' = \tau_o$. Thus,

$$\Delta V = K \bar{N} \left[\overline{\tau \tau_o} - \bar{\tau} \bar{\tau}_o \right] = K \bar{N} M \tag{7}$$

where M is the AC modulation.

As seen from Equation 5, the instrument signal, ΔV, may be increased by increasing the source radiance, $\bar{N}$, and by judicious selection of the transmission through the specifying cell, $\bar{\tau}_o$.

From this development, ΔV is proportional to $\bar{N}$, $\bar{\tau}_i$, and the overall responsivity and efficiency of the instrument. To eliminate these dependencies, a double-chopper system is used to facilitate an electronic ratioing technique. The signals generated by this system are shown schematically in Figure A-2.

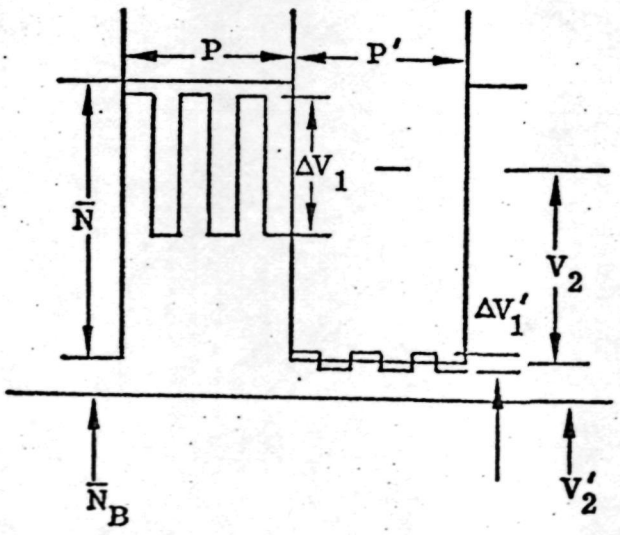

Figure A-2. Schematic diagram of signals generated by double-chopping GFC instrument.

Here we assume the source chopper, C_2, is operating at a lower frequency (f_2) than the instrument cell chopper, C_1. And we assume all background radiation, from the instrument or extraneous, is contained in the single term "$\bar{N}_B$." Then, the signals generated at frequency f_1 during phase P are given by

$$\Delta V_1 = (\bar{N} + \bar{N}_B)(\overline{\tau\tau}_o - \bar{\tau}\tau_r) + \bar{N}_{C_1}(\tau_r - \bar{\tau}_o) \tag{8}$$

where $\bar{N}_{C_1}$ is the radiance from chopper C_1 and the remaining symbols are as previously defined.

Similarly, during phase P′, when the source is blocked,

$$\Delta V_1' = (\bar{N}_B + \bar{N}_{C_2})(\overline{\tau\tau}_o - \bar{\tau}\tau_r) + \bar{N}_{C_1}(\tau_r - \bar{\tau}_o) \tag{9}$$

Now, $\Delta V_1 >> \Delta V_1'$, being proportional to the source radiance, so $\Delta V_1'$ is easily subtracted electronically from ΔV_1, giving

$$S_1 = \Delta V_1 - \Delta V_1' = (\bar{N} - \bar{N}_{C_2})(\overline{\tau\tau}_o - \bar{\tau}\tau_r) \tag{10}$$

The result is an AC signal at frequency f_1

The signals at frequency f_2 are similarly obtained. During P,

$$V_2 = (\bar{N} + \bar{N}_B)\left(\frac{\overline{\tau\tau}_o + \bar{\tau}\tau_r}{2}\right) + \bar{N}_{C_1}\left(\frac{\bar{\tau}_o + \tau_r}{2}\right) \tag{11}$$

and during P′,

$$V_2' = (\bar{N}_B + \bar{N}_{C_2})\left(\frac{\overline{\tau\tau}_o + \bar{\tau}\tau_r}{2}\right) + \bar{N}_{C_1}\left(\frac{\bar{\tau}_o + \tau_r}{2}\right) \tag{12}$$

Subtracting gives

$$S_2 = V_2 - V_2' = (\bar{N} - \bar{N}_{C_2})\left(\frac{\overline{\tau\tau}_o + \bar{\tau}\tau_r}{2}\right) \tag{13}$$

Forming the ratio between Equations 10 and 13 yields

$$\frac{S_1}{S_2} = 2\left(\frac{\overline{\tau\tau}_o - \bar{\tau}\tau_r}{\overline{\tau\tau}_o + \bar{\tau}\tau_r}\right) \tag{14}$$

This ratio is completely independent of all temperature-dependent instrument parameters, being a function only of the unknown transmissivity $\bar{\tau}$ and the instrument transmissivities $\bar{\tau}_o$ and τ_r. Thus, an extremely stable (no drift) signal results.

APPENDIX B

Post-Flight Diagnostic Tests

Subsequent to the operational flight, at the request of SAI the instrument was returned to the SAI lbaoratory in San Diego for diagnostic tests.

As a result of this investigation, several changes were made in the instrument data processing to improve its performance. Also, at this time, the corner cube retroreflector units in the wingtip-mounted array, which had been damaged during the flight, were replaced, and a new rotating gas cell was installed to replace the original cell which was found to be broken.

A discussion of each of these points follows. It would be valuable if, in future test flights, the "V" outputs, available on the front panel, were recorded in addition to the normal data outputs to assist in evaluating the performance.

System Noise

During the final tests of the instrument in December, 1975, prior to delivery to NASA, the noise levels were measured and reported to NASA personnel. Upon receipt, NASA personnel measured noise levels approximately five times higher than the pre-delivery measurements.

The original test tapes have been re-examined and it appears that an arithmetic error was made in the original data reduction. The pre-delivery noise was higher than reported by a factor of three, leaving a discrepancy of a factor of approximately 1.5, which is probably within the measurement accuracy.

Possible sources of this noise have been investigated.

The infrared detector vacuum jackets are intact. Loss of vacuum can be a source of S/N degradation if the capabilities of the thermoelectric cooler or its power supply are exceeded in trying to overcome the resulting air convection heat leakage. However, both detectors are being cooled to the original levels, as measured by the detector element resistance, with no increase in the thermoelectric cooler driving current.

The white noise generated by the electronic components is not the source of this residual system noise. This is easily demonstrated by optically blocking the detectors and observing the noise on the ΔV and V signals into the divider module (the divider module will not operate with zero voltage at the demominator input). Changes were made in the design of the preamps which further reduced this noise, but with negligible effect on the system noise level.

Numerous minor changes have been made, each contributing a corresponding improvement in noise level. A large portion of the remaining noise is believed to be due to tolerances in the rotating cell bearing and drive system and marginal torque on the chopper drive motor. These problems have been addressed on another program and if successful, should be retrofitted here.

By these efforts, the overall system noise on this instrument has now been reduced by a factor of 2 to 3. Because the sensitivity has also been affected by the changes made to improve the negative correlation phenomenon, the present noise-equivalent concentration is discussed at the end of the following section.

Negative Correlation Phenomenon

During the operational flight, the HCl and CO output signals exhibited the peculiar phenomenon of large random excursions which were mutually out of phase between the two channels. This can be seen in Figure 5-6.

These spurious signals could have been caused by a rapid change in the total IR radiant energy returning to the instrument, such as would be caused by rapid changes in the opacity of the atmosphere between the instrument window and the retroreflector. These laboratory tests have shown that such signals can be generated by this means.

The instrument data processing has been changed to reduce the sensitivity to rapid opacity variations. The electronics processing sequence is described in Section 4.2: synchronous demodulation of the 411 Hz V, signal, balance for $\Delta V=0$ by synchronous gain switching, and synchronous demodulation of the 9.1 Hz ΔV signal. The ratio $\Delta V/V$ is intended to remove the effect of radiance changes, but very short duration variations could enter the ΔV signal, instead of having proportional amplitudes. For these radiance pulses, the ratioing technique would fail. Because the HCl and CO channels use the same optical system, but with the gas-reference data mutually out of phase, a single radiance pulse would enter both channels with opposite polarity, as was observed in flight.

This effect has been reduced by a change in the demodulation of the 411 Hz signal. Previously, the sample-hold module sampled very narrow portions of the signal positive and negative peaks; this has been changed such that each now samples its entire half cycle and resistors in series with the hold capacitors cause the output to be averaged over all 411 Hz cycles occurring during each 180^{o} rotation of the gas cell. After the following differential amplifier, additional sample-hold module has been added which takes short samples at 9.1 Hz at such times that the charging interval of the averaging demodulator is removed. Thus, short duration radiance variations are severely attenuated before they enter the ΔV processing circuits.

By extending the sampling period to cover the entire half cycle, the output signal is reduced by approximately a factor of three compared to the previous peak-to-peak sampling, causing a corresponding factor of three degradation in the output signal-to-noise ratio. By improving the system noise level, the final noise-equivalent concentration, as discussed in the previous section, is similar to the pre-flight value for CO and is higher for HCl. These electronic changes are shown in Figure B-1.

Because the flight performance of the instrument was limited by the negative correlation phenomenon rather than system noise, a net improvement in field performance should result.

The final noise equivalent concentrations, expressed in terms of peak-to-peak noise and ppm concentration over a 10 meter path (2 pass, 5 meters each way) are:

Species	Time Constant	NEC, ppm	(Previous NEC)
HCl	0.5 sec	3.5	(2.0)
HCl	9 sec	0.82	(0.45)
CO	0.5 sec	0.61	(1.0)
CO	9 sec	0.14	(0.23)

Zero Offset

The data output zero offset which exists between data taken with the internal and the external retroreflectors was investigated. It is a function of the internal optical alignment of the instrument, but could not be eliminated within the existing adjustment ranges.

Gas Cell Repair

Upon initial disassembly of the instrument following receipt at the SAI laboratory, it was discovered that the Pyrex web, which separates the two halves of the rotating gas cell, was

cracked. Presumably, this was caused by handling shock or vibration acting on residual stress in the web. It is not known when the crack occurred, but no gas leakage apparently occurred since the instrument sensitivity was not affected.

The cracked cell was discarded and a new cell was constructed and installed.

Retroreflector Repair

The retroreflector array as installed on the wingtip tank shroud is shown in Figures 3-11, 5-2 and 5-3. The corner cubes making up the array are front surface aluminized and are installed with no protective window to prevent undersirable absorption or reflection. The array sensitive surfaces are thus, of necessity, exposed to any abrasive or corrosive environment.

The retroreflector was examined following the pre-launch test flight, 13 March 1976, at PAFB; no damage to the surface quality was seen.

However, following the operational flight, it was found that approximately 80% of the aluminum coating was destroyed, but with no apparent damage to the surface of the acrylic substrate. Presumably, this was caused by corrosive gases in the post-launch atmosphere. The retroreflector units (each is a sub-array of 60 corner cubes) are attached to the aluminum structure with RTV silastic and can be readily removed.

All damaged retroreflectors have been replaced with new units.

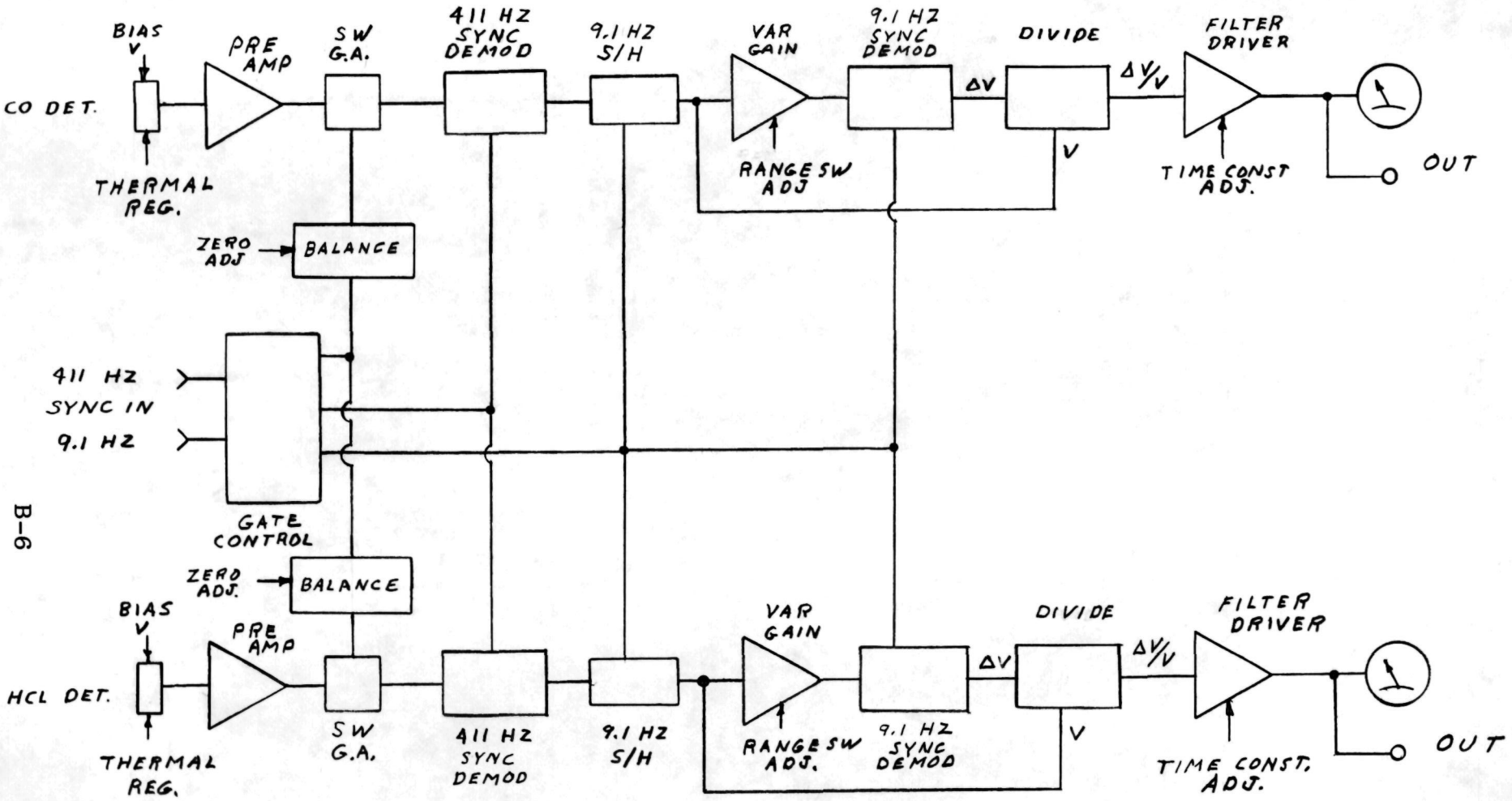

Figure B-1. Electronics Block Diagram (as revised).